Am J Physiol Heart Circ Physiol 305: H1761–H1771, 2013.
First published October 4, 2013; doi:10.1152/ajpheart.00159.2013.

Inhibition of NF-κB activation by a novel IKK inhibitor reduces the severity of experimental autoimmune myocarditis via suppression of T-cell activation

Ryo Watanabe,[1] Ryoko Wakizono Azuma,[2] Jun-ichi Suzuki,[3] Masahito Ogawa,[3] Akiko Itai,[4] Yasunobu Hirata,[3] Issei Komuro,[5] and Mitsuaki Isobe[1]

[1]*Department of Cardiovascular Medicine, Tokyo Medical and Dental University, Yushima, Bunkyo, Tokyo, Japan;* [2]*Department of Clinical Laboratory, Tokyo Medical and Dental University, Yushima, Bunkyo, Tokyo, Japan;* [3]*Department of Advanced Clinical Science and Therapeutics, University of Tokyo, Hongo, Bunkyo, Tokyo, Japan;* [4]*Institute of Medicinal Molecular Design, Hongo, Bunkyo-ku, Tokyo, Japan; and* [5]*Department of Cardiovascular Medicine, University of Tokyo, Hongo, Bunkyo, Tokyo, Japan*

Submitted 25 February 2013; accepted in final form 22 September 2013

Watanabe R, Azuma RW, Suzuki J, Ogawa M, Itai A, Hirata Y, Komuro I, Isobe M. Inhibition of NF-κB activation by a novel IKK inhibitor reduces the severity of experimental autoimmune myocarditis via suppression of T-cell activation. *Am J Physiol Heart Circ Physiol* 305: H1761–H1771, 2013. First published October 4, 2013; doi:10.1152/ajpheart.00159.2013.—NF-κB, which is activated by the inhibitor of NF-κB kinase (IKK), is involved in the progression of inflammatory disease. However, the effect of IKK inhibition on the progression of myocarditis is unknown. We examined the effect of IKK inhibition on the progression of myocarditis. Lewis rats were immunized with porcine cardiac myosin to induce experimental autoimmune myocarditis (EAM). We administered the IKK inhibitor (IMD-0354; 15 mg·kg^{-1}·day^{-1}) or vehicle to EAM rats daily. Hearts were harvested 21 days after immunization. Although the untreated EAM group showed increased heart weight-to-body weight ratio, and severe myocardial damage, these changes were attenuated in the IKK inhibitor-treated group. Moreover, IKK inhibitor administration significantly reduced NF-κB activation and mRNA expression of IFN-γ, IL-2, and monocyte chemoattractant protein-1 in myocardium compared with vehicle administration. In vitro study showed that the IKK inhibitor treatment inhibited T-cell proliferation and Th1 cytokines production induced by myosin stimulation. The IKK inhibitor ameliorated EAM by suppressing inflammatory reactions via suppression of T-cell activation.

myocarditis; inflammation; NF-κB kinase

ACUTE MYOCARDITIS IS A SERIOUS disease in humans; patients with myocarditis may suffer from rapidly progressive heart failure, shock, or severe arrhythmia. Although acute myocardial inflammation is an essential etiology for its progression, no effective treatment has been elucidated (3, 13, 30, 49). Because autoimmunity is important in myocarditis, a reaction to cardiac myosin may contribute to the development (14). In the pathology of myocarditis, T cells activated by antigen infiltrate into the myocardium, which may lead to myocardial damage by inflammatory reaction to myosin (23). Subsequently, the infiltration of CD4-positive T cells and macrophages into the myocardium promotes inflammatory reactions in the myocardium by releasing Th1 cytokines (e.g., IFN-γ and IL-2) (7) and chemokines [e.g., monocyte chemoattractant protein (MCP)-1] (11). NF-κB, which is regulated by NF-κB kinase (IKK), induces expression of genes that participate in the progression of inflammation (29, 41). Previously, we examined the effect of decoy oligonucleotide against NF-κB on ventricular remodeling after myocarditis (47). This report showed that NF-κB activity increased markedly in experimental autoimmune myocarditis (EAM) rat myocardium and that NF-κB is a key regulator in the progression of EAM. Activation of NF-κB induces gene programs that lead to transactivation of factors including Th1 cytokines and chemokines, promoting the inflammatory status involved in myocarditis (12, 16, 20, 38). Because NF-κB is the main factor in the development of inflammation, inhibition of its activation may be an effective therapy for myocarditis from the standpoint of preventing inflammation.

Recently, we developed IMD-0354, a novel inhibitor of IKK (19, 34, 41). This drug is a selective IKK-β inhibitor, blocks IκBα phosphorylation, and prevents NF-κB p65 nuclear translocation. Some previous studies reported the beneficial effects of IMD-0354 and its prodrug on inflammation-related cardiovascular diseases (15, 34, 35, 42). Therefore, regulation of NF-κB activation by the IKK inhibitor might have a potent effect on the treatment of myocarditis. However, the effect of IKK inhibitor treatment on the progression of myocarditis is unknown. Thus we assessed the hypothesis that IKK inhibitor treatment attenuates cardiac inflammation in the progression of myocarditis. EAM in a rat model is characterized by severe myocardial damage and multinucleated giant cell infiltration. This has been used as a disease model for human acute giant cell myocarditis (8). We examined the effect of IKK inhibition on EAM.

METHODS

Induction of EAM. Male Lewis rats (6-wk-old; body weights 150 to 200 g) were purchased from Charles River Laboratories Japan. They were fed a standard diet and water and were maintained in compliance with animal welfare guidelines of the Institute of Experimental Animals, Tokyo Medical and Dental University. Also, protocols were approved by the Institutional Animal Care and Use Committee of the Tokyo Medical and Dental University. Purified porcine cardiac myosin (Sigma Chemical, St. Louis, MO) was emulsified with an equal volume of complete Freund's adjuvant (Difco, Sparks, MD) supplemented with *Mycobacterium tuberculosis* H37RA (Disco) at a concentration of 10 mg/ml. On *day 0*, rats were injected in the footpads subcutaneously with 0.2 ml of emulsion, yielding an immunizing dose of 1.0 mg/body of cardiac myosin per rat (9) anesthetized by intraperitoneal administration of pentobarbital sodium (25 mg/kg; Dainihon Chemical, Osaka, Japan). We also used unimmunized (normal)

Address for reprint requests and other correspondence: J.-i. Suzuki, Dept. of Advanced Clinical Science and Therapeutics, Graduate School of Medicine, Univ. of Tokyo, 7-3-1 Hongo, Bunkyo-ku, Tokyo 113-8655, Japan (e-mail: junichisuzuki-circ@umin.ac.jp).

rats parallel with the diseased protocol. Unimmunized rats were injected saline instead of emulsion of myosin on *day 0*.

IKK inhibitor administration. The IKK inhibitor IMD-0354 was provided by the Institute of Medicinal Molecular Design. The drug was dissolved in 0.5% carboxy methyl cellulose (CMC) solution immediately before use. In the EAM phase, cardiac inflammation starts on approximately *day 14*, and the peak of inflammation is expected to occur on *day 21* (25). For this reason, we administered the IKK inhibitor either from *day 1* or from *day 14*, and harvested hearts and spleens on *day 21*. Rats were assigned randomly to five groups: *1*) daily CMC intraperitoneal injection to normal rats from *day 1* to *day 20* [normal + vehicle group; $n = 6$], *2*) daily IMD-0354 intraperitoneal injection (15 $mg \cdot kg^{-1} \cdot day^{-1}$) to normal rats from *day 1* to *day 20* [normal + IKKi(1–20); $n = 5$], *3*) daily CMC intraperitoneal injection to EAM rats from *day 1* to *day 20* [EAM + vehicle; $n = 18$], *4*) daily IMD-0354 intraperitoneal injection (15 $mg \cdot kg^{-1} \cdot day^{-1}$) to EAM rats from *day 1* to *day 20* [EAM + IKKi(1–20); $n = 13$], and *5*) daily IMD-0354 intraperitoneal injection (15 $mg \cdot kg^{-1} \cdot day^{-1}$) to EAM rats from *day 14* to *day 20* [EAM + IKKi(14–20); $n = 10$]. Administration dose of the IKK inhibitor was calculated from that of previous articles (17, 19, 31, 34, 35).

Echocardiogram. Transthoracic echocardiography was performed on animals anesthetized by intraperitoneal administration of pentobarbital sodium (25 mg/kg) on *day 21*. An echocardiography machine with a 7.5-MHz transducer (Nemio; Toshiba, Tokyo, Japan) was used for M-mode left ventricular (LV) echocardiographic recording. A two-dimensional targeted M-mode echocardiogram was obtained along the short-axis view of the LV papillary muscles (40). LV posterior wall thickness at diastole (LVPWd), interventricular septal thickness at diastole (IVSTd), and percent ejection fraction (EF) were calculated from the M-mode recordings.

Histopathological examination. Hearts and spleens were harvested immediately after all rats were killed by the cutting of the abdominal aorta under anesthesia after the echocardiographic examination on *day 21*. After heart weights were measured, hearts were divided into apex, midventricular, and basal level slices. Apex level slice was frozen by liquid nitrogen, and it was stored at −80°C until before use. This slice was used as the sample for Western blotting or real-time RT-PCR. Midventricular level slices and spleens were fixed by formalin or embedded by optimum cutting temperature compound (Sakura Finetek, Tokyo, Japan). OCT compound-embedded slices were frozen by liquid nitrogen. These slices were used for histopathological or immunohistochemical examination. Formaldehyde-fixed paraffin sections were stained with hematoxylin and eosin or the Mallory method. The extent of inflammatory cell infiltration and myocardial necrosis was estimated using hematoxylin and eosin staining. The degree of fibrosis was estimated using Mallory staining. The cell infiltration area ratio (cell infiltration area/total area expressed as a percentage) and the fibrosis area ratio (the Mallory stained area/total area expressed as a percentage) were calculated by a computer-assisted analyzer (Scion Image beta 4.0.2) as described previously (1, 9, 28).

Immunohistochemistry. Immunohistochemistry was performed to detect CD4- or CD8-positive T cells, macrophages, NF-κB p65, and phospho-NF-κB p65 in the heart or the spleen on *day 21*. Paraffin or frozen sections were incubated with primary antibodies against CD4 (10B5; Abcam, Cambridge, UK), CD8 (OX8; BD PharMingen California), CD68 (as a marker of macrophage; ED1; Santa Cruz Biotechnology, Santa Cruz, CA), and NF-κB p65 (Abcam) for 8 h at 4°C and washed in PBS followed by biotinylated secondary antibodies (Nichirei, Tokyo, Japan) at 5 mg/ml for 30 min at room temperature. Finally, each section was reacted with AEC (aminoethylcarbazole complex) solution (Nichirei) for 5 to 30 min. Sections were counterstained with hematoxylin solution. We counted the number of positive cells against CD4, CD8, and CD68 in randomly selected five random microscopical fields (original magnification, ×200) per sample section, and averaged it (10). Immunofluorescence double staining was performed to identify colocalization of CD4 positive cells and phospho-NF-κB p65 in the heart and spleen. Antibodies against CD4 (OX35; mouse- monoclonal; Abcam) and phospho-NF-κB p65 (Ser536; 93H1; rabbit- monoclonal; Cell Signaling Technology) were co-incubated and detected with Alexa 488 anti-mouse antibody (Life Technologies Japan) and Alexa 568 anti-rabbit antibody (Life Technologies), respectively. Nuclei were stained with 4′,6-diamidino-2-phenylindole.

Extraction of proteins from hearts. To extract tissue protein, frozen cardiac tissues from an apex level heart slice was homogenized in lysis buffer of 50 mM Tris·HCl (pH 7.5), 150 mM NaCl, 1% Triton X-100, 2 mM EGTA, 10 mM EDTA, 100 nM NaF containing protease inhibitor cocktail tablets (Roche Diagnostic, Basel, Switzerland) and phosphatase inhibitor cocktail tablets (Roche Diagnostic). Nuclear and cytosolic proteins were isolated from frozen cardiac tissues from the same apex level heart slice using Nuclear Extraction Kit (Epigentek Group). Protein concentrations were measured with a BCA protein assay (Bio-Rad, Milan, Italy) to equalize the protein concentrations of all samples. Protein samples were stored at −80°C until they were used.

Western blotting. Equal amounts of proteins were separated by SDS-PAGE, transferred to a nitrocellulose membrane, and incubated overnight with antibodies to IκB (Abcam), phospho-IκB (Cell Signaling Technology), GAPDH (Cell Signaling Technology), NF-κB p65 (Abcam), phospho-NF-κB p65 (Ser536; Cell Signaling Technology), and Lamin A/C (Cell Signaling Technology) at 4°C. The membranes were incubated with a secondary antibody (Amersham Biosciences, Piscataway, NJ) for 2 h and developed with ECL reagent (Amersham Biosciences). Enhanced chemiluminescence was detected with an LAS-1000 (Fujifilm, Tokyo, Japan). The value was calculated using ImageJ [National Institutes of Health (NIH)].

Real-time RT-PCR. Total RNA was isolated from frozen apex level heart slice tissues using TRIsure (Bioline, London, UK), and cDNA was prepared with the high capacity cDNA Reverse Transcription Kit (Applied Biosystems). Real-time PCR in a Step One real-time PCR system (Applied Biosystems) was used to determine the mRNA expression of IFN-γ (Assay ID: Rn99999014_m1), IL-2 (Assay ID: Rn00587673_m1), and MCP-1 (Assay ID: Rn00580555_m1) and 18s rRNA (Assay ID: Hs99999901_s1) as a control. cDNA was run in duplicates, quantitative data were calculated using the comparative

Table 1. *Echocardiographic parameters*

	n	LV Diameter at Diastole, mm	LV Diameter at Systole, mm	Ejection Fraction, %	Interventricular Septal Thickness at Diastole, mm	LV Posterior Wall Thickness at Diastole, mm
Normal + vehicle	6	6.3 ± 0.26	3.0 ± 0.17	89 ± 0.5	1.8 ± 0.16	2.2 ± 0.22
Normal + IKKi(1–20)	5	6.5 ± 0.21	3.4 ± 0.09	85 ± 1.4	1.6 ± 0.09	2.1 ± 0.35
EAM + vehicle	11	6.0 ± 0.28	3.6 ± 0.33	75 ± 4.7	2.5 ± 0.20#	2.9 ± 0.29
EAM + IKKi(1–20)	12	6.6 ± 0.15	4.0 ± 0.27	76 ± 3.9	1.7 ± 0.11*	1.9 ± 0.12*
EAM + IKKi(14–20)	7	6.1 ± 0.11	3.8 ± 0.16	74 ± 2.2	1.6 ± 0.09*	2.5 ± 0.14

Values are means ± SE. Early IKK inhibitor treatment [experimental autoimmune myocarditis (EAM) + IKKi(1–20)] suppressed an increase of interventricular septal thickness at diastole and left ventricular (LV) posterior wall thickness at diastole values, whereas late IKK inhibitor treatment [EAM + IKKi (14–20)] only suppressed an increase of interventricular septal thickness at diastole value compared with vehicle treatment [EAM + vehicle] on *day 21*. #$P < 0.05$ vs. normal + vehicle; *$P < 0.05$ vs. EAM + vehicle.

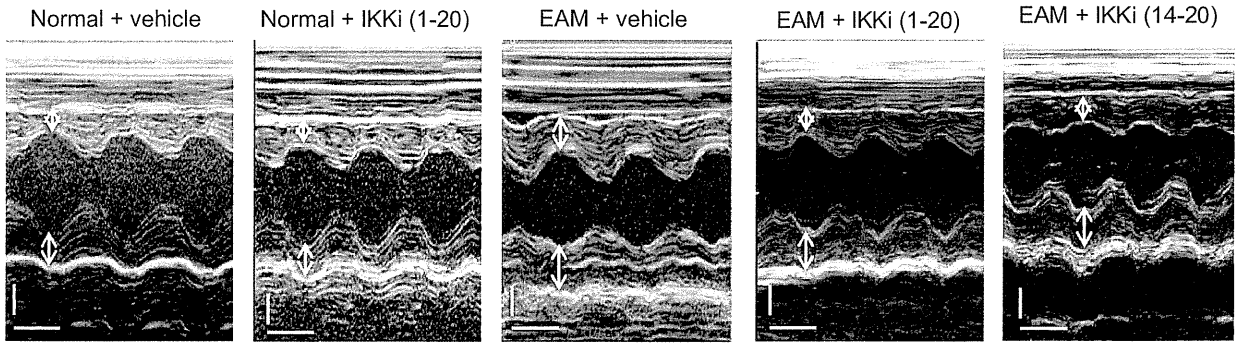

Fig. 1. Representative M-mode echocardiograms on *day 21*. Arrows indicate anterior and posterior walls of left ventricle. Scale bars: 2 millimeter (vertical) and 0.1 s (horizontal).

CT ($\Delta\Delta C_T$) method, and the mRNA expression was normalized by normal rat hearts (28, 32).

T-cell proliferation assay. Cells were isolated from spleen in the EAM + vehicle group on *day 21*. Cells (5×10^6/well) were cultured in 96-well culture plates with 50 μg/ml purified porcine heart myosin. The IKK inhibitor was added to each well at various concentrations. In vitro dosage of the IKK inhibitor was determined according to that in previous articles (34, 35). Cultures were incubated at 37°C under 5% CO_2 for 3 days. Cells were centrifuged at 1,200 rpm for 5 min, and the supernatants were stored at −80°C until before use. T-cell proliferation was assessed with the Cell Counting Kit-8 (Dojindo, Tokyo, Japan) with the use of cells of the precipitation. Cell proliferation was expressed as the optical density (9).

Enzyme-linked immunosorbent assay. We performed enzyme-linked immunosorbent assay (ELISA) to examine the production of Th1 cytokines from T cells using the supernatants of cell culture in T-cell proliferation assays. Concentrations of IFN-γ and IL-2 in cell culture supernatant were determined with the Rat IL-2 quantikine ELISA kit (R & D Systems, Minneapolis, MN) and rat IFN-γ ELISA KIT (Gen-Probe, San Diego, CA) according to the manufacturer's instructions.

Statistical analysis. All data are expressed as means ± SE. Statistical analyses were performed with statistical software (Stat View; SAS Institute). Student's *t*-test was used to compare data between the two groups. Data differences between multiple groups were subjected to ANOVA followed by a Bonferroni-Dunn test. Differences were considered statistically significant at a value of $P < 0.05$.

RESULTS

Echocardiographic parameters. On *day 21*, the values of LV diameter at diastole, LV diameter at systole, and EF did not show any statistical difference among all groups. Regarding IVSTd and LVPWd values, no significant difference was observed between the normal + vehicle group and the normal + IKKi(1–20) group. IVSTd values significantly increased in the EAM + vehicle group compared with the normal + vehicle group. IVSTd and LVPWd values in the EAM + IKKi(1–20) group were reduced compared with those of the EAM + vehicle group. Additionally, IVSTd value was reduced in the EAM + IKKi(14–20) group compared with that of the EAM + vehicle group, although LVPWd value was not changed. There was no significant difference regarding IVSTd and LVPWd values between the EAM + IKKi(14–20) group and the EAM + IKKi(1–20) group (Table 1 and Fig. 1).

The IKK inhibitor suppressed heart weight gain by cardiac inflammation. The normal + IKKi(1–20) group did not show any change in heart weight compared with the normal + vehicle group. The EAM + vehicle group hearts demonstrated an increase of the heart-to-body weight ratio compared with that of the normal + vehicle group. This ratio in the EAM + IKKi(1–20) group was significantly smaller than that of the EAM + vehicle group, whereas the EAM + IKKi(14–20) group was not statistically different compared with the EAM + vehicle group. There was no significant difference of this ratio between the EAM + IKKi(14–20) group and the EAM + IKKi(1–20) group (Fig. 2).

The IKK inhibitor reduced myocardial damage characterized by cell infiltration and fibrosis in EAM. Histopathologically, the heart of the EAM + vehicle group showed severe myocarditis lesions that were composed of extensive inflammatory cell infiltration and myocardial fibrosis on *day 21*. However, the cell infiltration area ratios in the EAM + IKKi(1–20) group (12.9 ± 3.6%; $P < 0.05$) and the EAM + IKKi(14–20) group (22.5 ± 2.9%; $P < 0.05$) were significantly fewer than those in the EAM + vehicle group (36.5 ± 3.4%) (Fig. 3, *A–C*). Similarly, the fibrosis area ratios in the EAM + IKKi(1–20) group (15.8 ± 4.0%; $P < 0.05$) and the EAM + IKKi(14–20) group (21.4 ±

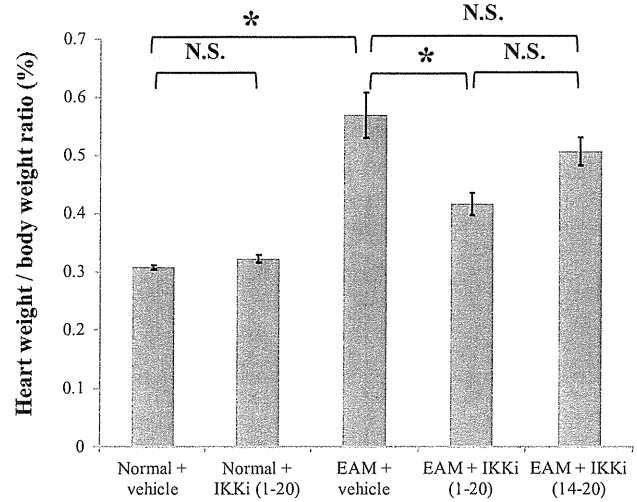

Fig. 2. Heart-to-body weight ratio. The experimental autoimmune myocarditis (EAM) + IKKi(1–20) group had a smaller the heart-to-body weight ratio than the EAM + vehicle group. The EAM + IKKi(14–20) group did not show the effect of the heart-to-body weight ratio compared with that of the EAM + vehicle group on *day 21* [normal + vehicle, $n = 5$; normal + IKKi(1–20), $n = 5$; EAM + vehicle, $n = 12$; EAM + IKKi(1–20), $n = 12$; EAM + IKKi(14–20), $n = 10$]. *$P < 0.05$. NS, not significant.

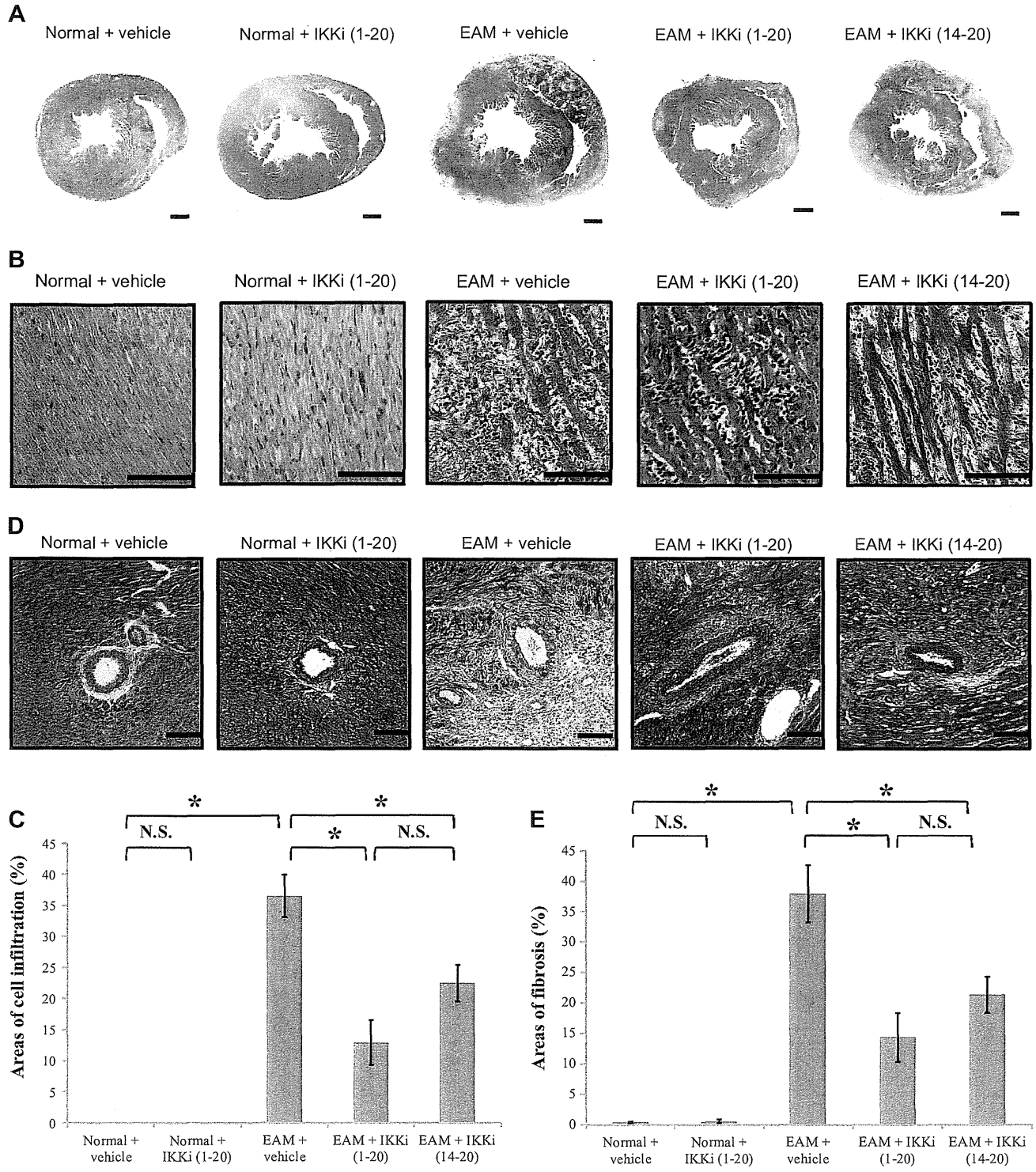

Fig. 3. Histopathological findings. Representative low-power (magnification, ×10; scale bars = 1 millimeter; *A*) and high-power (magnification, ×400; scale bars = 100 μm; *B*) photomicrographs of hematoxylin and eosin-stained cross-sections are shown. *C*: quantitative data of cell infiltration area. IKK inhibitor treatment significantly suppressed cell infiltration into myocardium on *day 21* [normal + vehicle, $n = 5$; normal + IKKi(1–20), $n = 5$; EAM + vehicle, $n = 14$; EAM + IKKi(1–20), $n = 12$; EAM + IKKi(14–20), $n = 10$]. $^*P < 0.05$. *D*: representative photomicrographs (magnification, ×200; scale bars = 100 μm) of Mallory-stained cross-sections. *E*: quantitative data of fibrosis area. IKK inhibitor treatment significantly suppressed cardiac fibrosis on *day 21* [normal + vehicle, $n = 5$; normal + IKKi(1–20), $n = 5$; EAM + vehicle, $n = 14$; EAM + IKKi(1–20), $n = 12$; EAM + IKKi(14–20), $n = 10$]. $^*P < 0.05$.

2.9%; $P < 0.05$) were significantly lower than those in the EAM + vehicle group (37.9 ± 4.7%), respectively (Fig. 3, *D* and *E*). There was no significant difference regarding these histopathological changes between the EAM + IKKi(1–20) group and the EAM + IKKi(14–20) group. Hearts from the normal + IKKi(1–20) group did not show abnormal histopathological change compared with the normal + vehicle group.

The IKK inhibitor attenuated inflammatory cell infiltration in EAM hearts. After histopathological examination, we analyzed the effect of IKK inhibitor treatment on each inflammatory infiltrating cell. Hearts from the EAM + vehicle group showed massive infiltrations of CD-4 positive T cells and CD68-positive macrophages, and moderate infiltration of CD8-positive T cells on *day 21*. However, the EAM + IKKi(1–20) group showed significant reductions of CD4-, CD8-, and CD68-positive cell numbers compared with the EAM + vehicle group (Fig. 4, *A–D*).

Localization of NF-κB activation in EAM. To investigate NF-κB activity in EAM, we performed immunohistochemical analysis. On *day 21*, NF-κB p65 was expressed in the cytoplasm of cardiac tissues from the normal + vehicle group. In contrast, strong expression of NF-κB p65 was observed mainly in the nucleus of the infiltrating cells in the myocardium as shown by arrows in the hearts from the EAM + vehicle group (Fig. 5*A*). On this occasion, NF-κB p65 phosphorylation (as a marker of NF-κB activation) was detected in CD4-positive T cells that infiltrated the myocardium in the EAM + vehicle group (Fig. 5*B*). CD4-positive T cells play a critical role in the development of EAM. The spleen is a major source of immune cells, including CD4-positive T cells. Immune cells derived from the spleen migrate to the inflammatory affected area through the blood stream (37). Hence, we examined NF-κB activation in the spleen during the development of EAM. In the spleen obtained from the EAM + vehicle group, we observed enhanced colocalization of phospho-NF-κB p65 and CD4-positive T cells compared with that of the normal + vehicle group (Fig. 5*C*).

IKK inhibitor suppressed NF-κB activation in EAM hearts. To examine the effect of IKK inhibitor treatment on NF-κB activity in the heart of EAM, we analyzed nuclear NF-κB p65 protein expression, NF-κB p65 phosphorylation level, and cytosolic phospho-IκB-to-IκB ratio (35). The EAM + vehicle group showed enhanced nuclear NF-κB p65 protein expression compared with the normal + vehicle group. However, nuclear NF-κB p65 protein expression was significantly reduced in the EAM + IKKi(1–20) group compared with the EAM + vehicle group on *day 21* (Fig. 6, *A* and *B*). Phosphorylation level of NF-κB p65 (as shown by phospho-NF-κB-to-total NF-κB ratio) was reduced by IKK inhibitor administration (Fig. 6, *C* and *D*). Moreover, the level of cytosolic phospho-IκBα-to-IκB

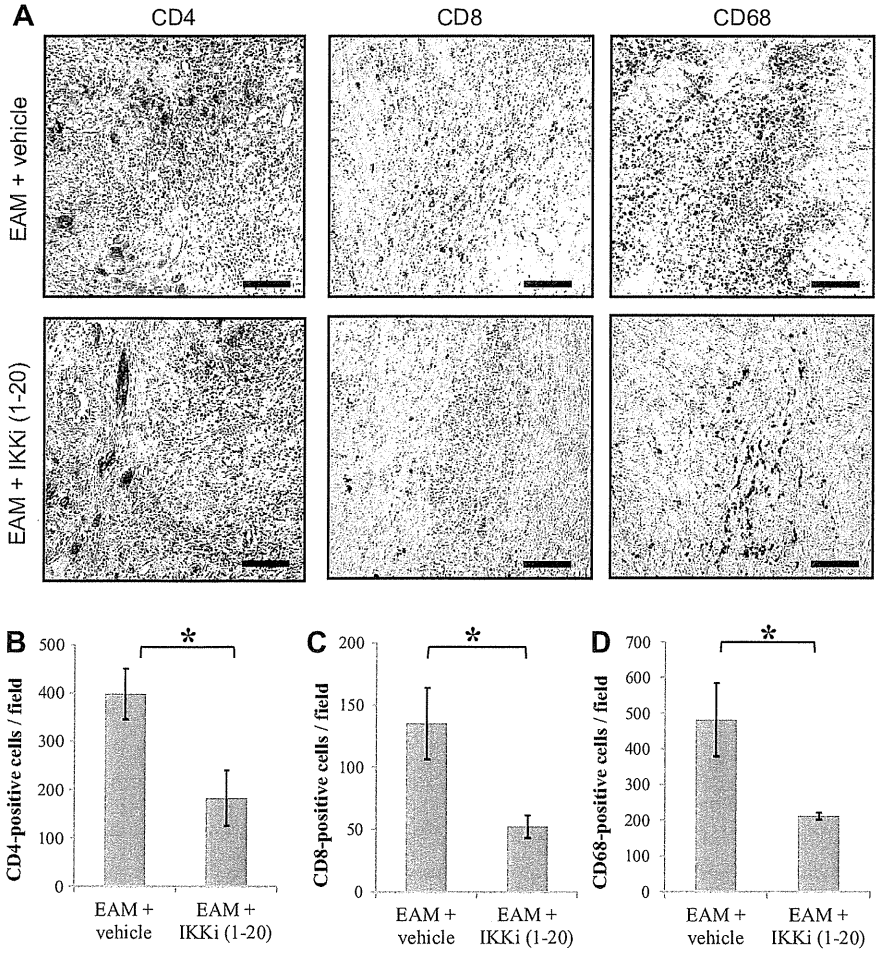

Fig. 4. Infiltrations of inflammation-related cells on *day 21*. *A*: representative CD4 staining, CD8 staining, and CD68 staining photomicrographs (magnification, ×200; scale bars = 100 μm). Quantitative results of immunohistochemistry for CD4-positive T cell [EAM + vehicle, $n = 8$; EAM + IKKi(1–20), $n = 7$; *B*], CD8-positive T cell [EAM + vehicle, $n = 7$; EAM + IKKi(1–20), $n = 8$; *C*], and CD68-positive macrophage [EAM + vehicle, $n = 7$; EAM + IKKi(1–20), $n = 6$; *D*] are shown. IKK inhibitor treatment reduced numbers of CD4-, CD8-, and CD68-positive infiltrating cells in EAM hearts on *day 21*. *$P < 0.05$.

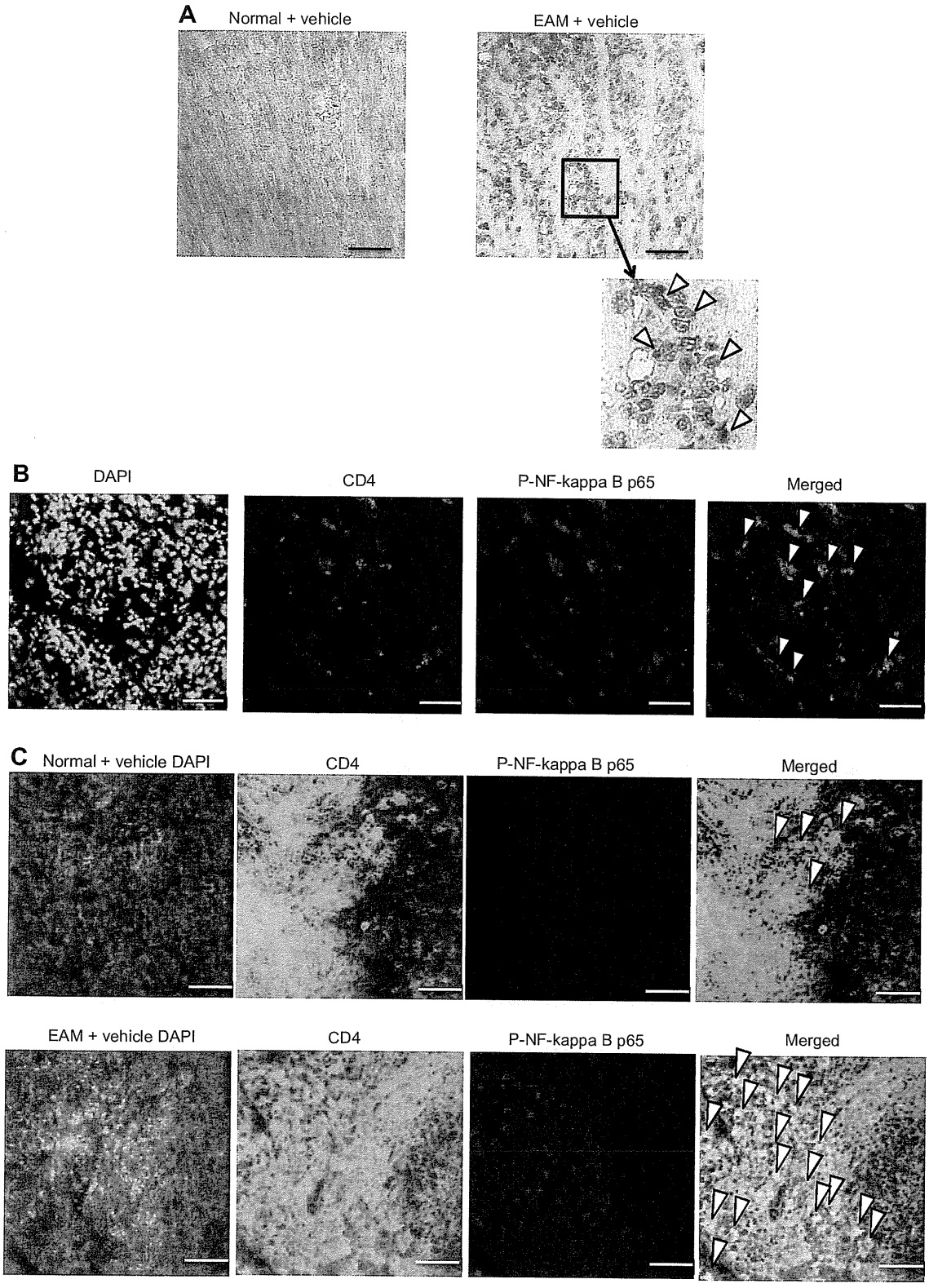
A
Normal + vehicle
EAM + vehicle
B
DAPI
CD4
P-NF-kappa B p65
Merged
C
Normal + vehicle DAPI
CD4
P-NF-kappa B p65
Merged
EAM + vehicle DAPI
CD4
P-NF-kappa B p65
Merged

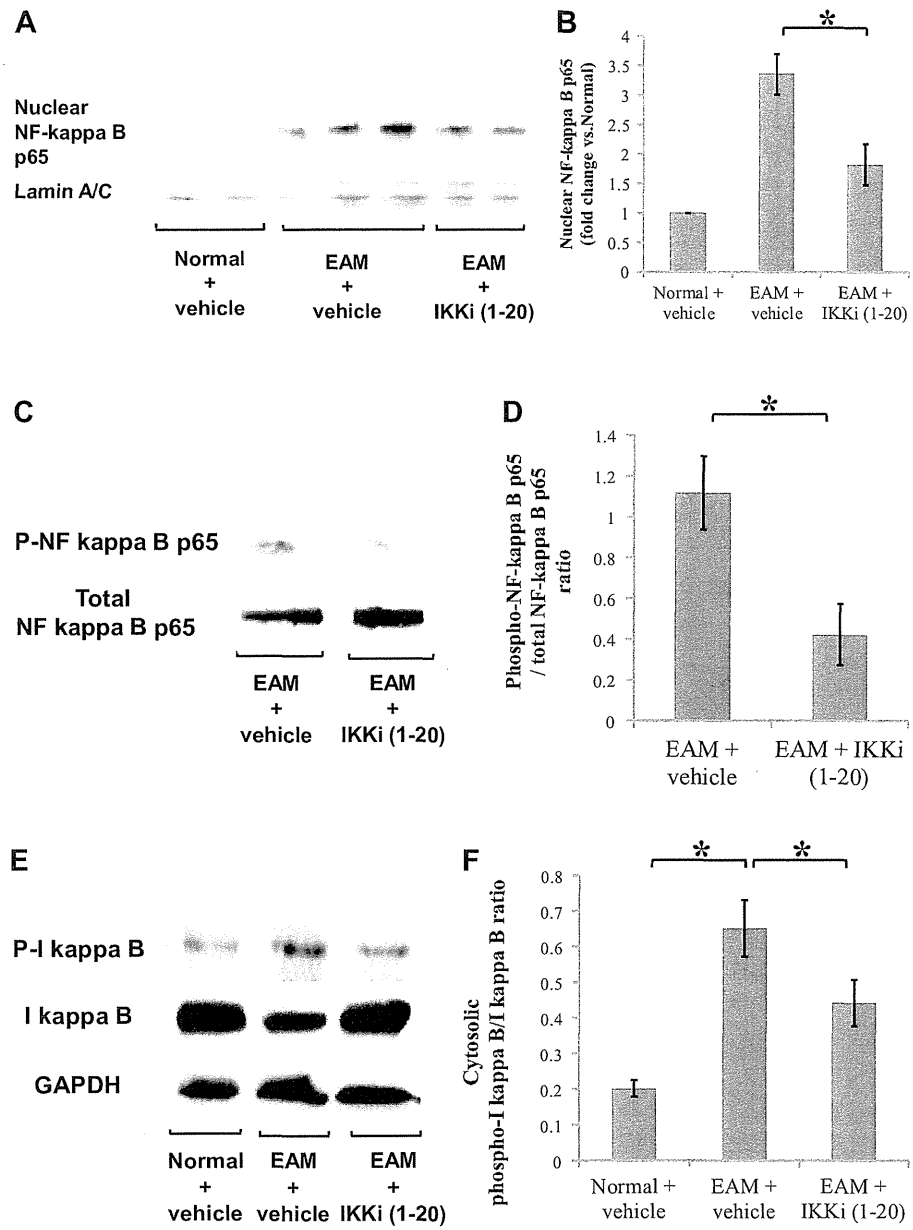

Fig. 6. Activity of NF-κB in each group on *day 21*. *A*: results of representative Western blotting for nuclear NF-κB p65 and lamin A/C. *B*: relative quantitative results of NF-κB p65 nuclear translocation [normal + vehicle, $n = 3$; EAM + vehicle, $n = 5$; EAM + IKKi(1–20), $n = 4$]. *C*: results of representative Western blotting for phospho-NF-κB p65 and total-NF-κB p65. *D*: quantitative results of phospho-NF-κB p65-to-total-NF-κB p65 ratio (as an index of NF-κB p65 phosphorylation) [EAM + vehicle, $n = 4$; EAM + IKKi(1–20), $n = 4$]. *E*: results of representative Western blotting for cytosolic IκBα, phospho-IκBα, and GAPDH. *F*: quantitative results of cytosolic phospho-IκBα-to-IκBα ratio (as an index of IκBα phosphorylation) [normal + vehicle, $n = 6$; EAM + vehicle, $n = 11$; EAM + IKKi(1–20), $n = 8$]. IKK inhibitor administration suppressed NF-κB activation in EAM hearts tissue. $^*P < 0.05$.

ratio in EAM hearts increased in the EAM + vehicle group compared with the normal + vehicle group. However, it decreased by IKK inhibitor administration (Fig. 6, *E* and *F*).

Altered inflammation-related gene expression by IKK inhibition in EAM hearts. Th1 cytokines and chemokines are known to promote myocardial inflammation during EAM (7, 11). Therefore, we examined the effect of IKK inhibitor treatment on mRNA expression of a chemokine and Th1 cytokines in hearts on *day 21* using real-time RT-PCR. In the EAM + vehicle group, mRNA expressions of IFN-γ, IL-2, and MCP-1 were enhanced compared with the normal + vehicle group. However, mRNA expressions of these genes were significantly suppressed in the EAM +

Fig. 5. Localization of NF-κB activation in EAM on *day 21*. *A*: representative immunohistochemistry of hearts from the normal + vehicle group and the EAM + vehicle group (magnification, ×400; scale bars = 50 μm). In EAM hearts (EAM + vehicle), NF-κB p65 was expressed in the nucleus of infiltrating cells (as shown by arrows). *B*: representative immunofluorescence double staining findings of the myocardium in the EAM + vehicle group on *day 21* (magnification, ×400; scale bars = 50 μm). Phospho (P)-NF-κB p65 was detected on CD4-positive infiltrating cells (as shown by arrows) in the EAM + vehicle group. *C*: representative immunofluorescence double staining findings of the spleen from the normal + vehicle group and the EAM + vehicle group on *day 21* (magnification, ×400; scale bars = 50 μm). Colocalization of phospho-NF-κB p65 and CD4-positive cells (as shown by arrows) were observed in the spleens from the EAM + vehicle group. DAPI, 4′,6-diamidino-2-phenylindole.

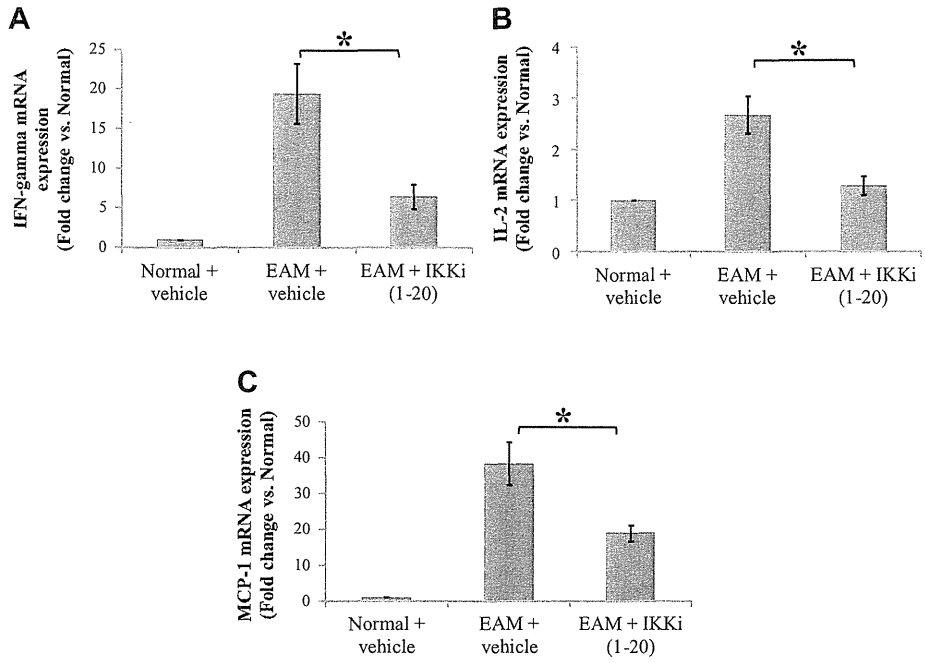

Fig. 7. mRNA expression of inflammation-related genes. Results of real-time RT-PCR for IFN-γ (*A*), IL-2 (*B*), and monocyte chemoattractant protein (MCP-1; *C*). IKK inhibitor treatment significantly suppressed mRNA expressions of IFN-γ, IL-2, and MCP-1 on *day 21* [normal + vehicle, $n = 3$; EAM + vehicle, $n = 12$; EAM + IKKi(1–20), $n = 9$]. *$P < 0.05$.

IKKi(1–20) group compared with the EAM + vehicle group (Fig. 7, *A–C*).

Suppression of antigen-induced T-cell proliferation by IKK inhibitor treatment. Our present study revealed that NF-κB activation was observed in CD4-positive T cells in the heart and spleen during the development of EAM. Additionally, previous studies reported that EAM is transferable to other individuals via T cells derived from the spleen of EAM (21, 46). T cells activated by antigen mediate the development of EAM. Therefore, we performed a T-cell proliferation assay to examine the effect of IKK inhibitor on antigen-induced T-cell proliferation using splenocytes of EAM. As a result, T-cell proliferation was significantly increased by myosin restimulation. IKK inhibitor treatment suppressed myosin-induced T-cell proliferation in a dose-dependent manner (Fig. 8).

Effect of IKK inhibitor on the production of Th1 cytokines in vitro. It is known that Th1 cytokines released from CD4-positive T cells mediate the progression of EAM (33). Thus, to examine the effects of IKK inhibitor on the production of Th1 cytokines from T cells activated by antigen, we performed ELISA using supernatants collected from T-cell proliferation assays. In consequence, productions of IFN-γ and IL-2 were significantly increased by myosin restimulation. However, IKK inhibitor treatment suppressed the production of these th1 cytokines in a dose-dependent manner (Fig. 9, *A* and *B*).

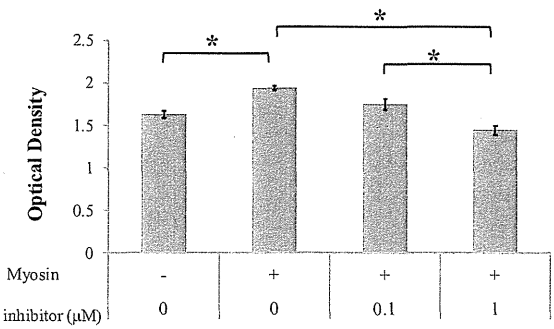

Fig. 8. The effect of IKK inhibitor treatment on antigen-induced T-cell proliferation. The IKK inhibitor suppressed antigen-induced T-cell proliferation in a dose-dependent manner ($n = 10$ each). *$P < 0.05$.

DISCUSSION

NF-κB is a key factor for the progression of inflammation (35, 47). Our previous articles showed that inhibition of NF-κB activation by the IKK inhibitor significantly suppressed pro-inflammatory mediators in myocardial ischemia model (34, 45). Inflammation is an essential pathological feature of acute myocarditis. Although the effectiveness of the IKK inhibitor on cardiac diseases associated with inflammation was shown, the effect of the IKK inhibitor on myocarditis remains unknown.

IKK inhibitor treatment did not change the value of EF compared with vehicle treatment on *day 21*. However, the EAM + IKKi(1–20) group exhibited an antihypertrophic effect, as shown by suppression of increases of LVPWd and IVSTd values. This effect was consistent with the result that IKK inhibitor treatment suppressed heart weight gain. The increased wall thickness is considered to be owing to interstitial edema associated with progression of myocardial inflammation. In contrast, the EAM + IKKi(14–20) group suppressed the increase of IVSTd value; however, it did not affect LVPWd value and heart weight gain. Earlier IKK inhibitor treatment may be more effective. The severity of histological myocardial damage characterized by cell infiltration and fibrosis was significantly reduced in both the EAM + IKKi(14–20) group and the EAM + IKKi(1–20) group compared with the EAM + vehicle group. Additionally, it should be noted that there was no significant difference regarding this effect between the EAM + IKKi(14–20) group and the EAM +

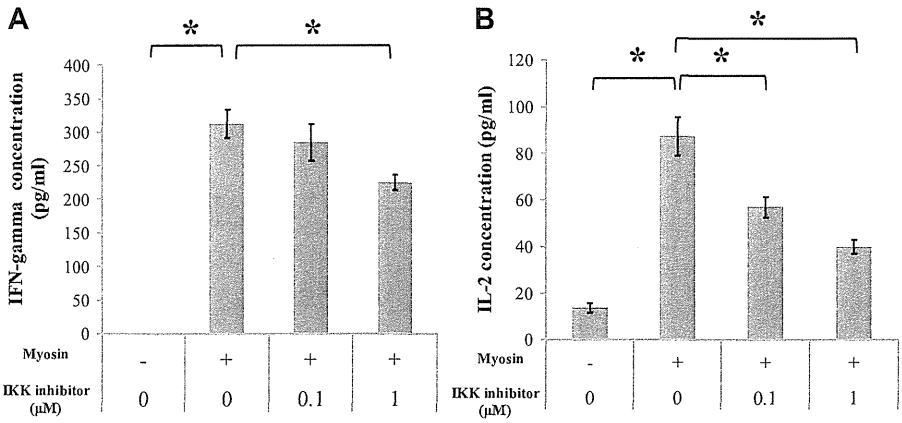

Fig. 9. The effect of IKK inhibitor treatment on antigen-induced production of Th1 cytokines. Results of enzyme-linked immunosorbent assay for IFN-γ (*A*) and IL-2 (*B*) are shown. The production of Th1-type cytokines, including IFN-γ (n = 10 each) and IL-2 (n = 10 each), was significantly reduced by IKK inhibitor administration in vitro. *$P < 0.05$.

IKKi(1–20) group. We revealed that even when IKK inhibitor administration began from *day 14*, IKK inhibitor treatment suppressed myocardial damage and it was not inferior to the early IKK inhibitor treatment group [EAM + IKKi(1–20)]. Thus our results suggest that the treatment effect of IMD-0354 was due to the suppression of the inflammatory reaction that was caused around *day 14*. In a clinical setting, time lag occurs before patients are diagnosed with myocarditis and receive medical treatment. Therefore, IKK inhibitor treatment from *day 14* to *day 21* [EAM + IKKi(14–20)] was a trial to inspect utility as a therapeutic medicine of myocarditis. Meanwhile, there was no significant difference in echocardiographic parameters and histopathological findings between the normal + vehicle group and the normal + IKKi(1–20) group. These results suggest that the IKK inhibitor IMD-0354 does not affect normal hearts.

We observed massive infiltrations of CD4-positive T cells and CD68-positive macrophages, and moderate infiltration of CD8-positive T cells in the EAM + vehicle group hearts tissue. Infiltration cells into myocardium consist of mainly macrophages and CD4-positive T cells in EAM, and this result is consistent with those of previous studies (14, 22). These inflammatory cell infiltrations were suppressed by IKK inhibitor administration. NF-κB induces activation of inflammatory cells such as T cells and macrophages (2, 18). During the inflammatory phase of EAM, Th1 cytokines are enhanced and they mediate interaction between CD4-positive T cells and macrophages, which lead to cardiac damages (8, 14, 33). In particular, CD4-positive T cells proliferate oneself by releasing IL-2 and activate macrophages by releasing IFN-γ. Subsequently, activating macrophages damage myocardium (33). MCP-1 is known as a chemotactic factor and plays essential role in the inflammatory reaction involved in the progress of myocarditis by having an influence on the recruitment of inflammatory cells (11). Many inflammation-related genes including IFN-γ, IL-2, and MCP-1 are expressed by NF-κB (5, 43, 44), and its suppression prevents the development of EAM (11, 27, 36). Our in vivo studies revealed that mRNA expression of IFN-γ, IL-2, and MCP-1 were suppressed by IKK inhibitor treatment through inhibition of NF-κB activation in EAM heart tissues. Therefore, inhibition of NF-κB activation by IKK inhibitor treatment to suppress expression of inflammation-related genes may prevent harmful inflammatory cell infiltration in myocarditis.

In the process of EAM, CD4-positive T cells were activated by cardiac myosin and then recruited to the target organ (heart) (39). It is known that this cell play a particularly significant role in the pathophysiology of EAM. We demonstrated that NF-κB activation was observed mainly in CD4-positive T cells infiltrating the myocardium in EAM. A major source of inflammatory cells, including CD4-positive T cells, is the spleen (37). Therefore, we examined NF-κB activity in CD4-positive T cells of the spleen during EAM. We also detected NF-κB activation of CD4-positive T cells in spleens in EAM. A recent study reported that immune cells derived from the spleen reach the myocardium via the blood stream and induced inflammatory reaction during inflammation-related cardiac disease (24). Moreover, some previous studies reported that splenocytes play a role of the pathogen and transferred myocarditis (21, 26, 46). Therefore, we investigated the direct effects of the IKK inhibitor on T cells, which were activated by antigen and derived from the spleen. Our in vitro study revealed that IKK inhibitor treatment suppressed myosin induced T-cell proliferation and production of Th1 cytokines. NF-κB activation is necessary for T-cell activation, differentiation, and proliferation (4). Activated T cells secrete various cytokines and chemokines via NF-κB activation, which activate other inflammatory cells or cardiomyocytes in the myocardium and cause further recruitment of inflammatory cells (34, 48). Antigen-induced T-cell proliferation and subsequent production of Th1 cytokines from T cells are an essential response for the development of EAM (8). This evidence demonstrates that the IKK inhibitor suppressed the activation of T cells and attenuated the development of EAM. Therefore, our results suggested that IMD-0354 attenuated the severity of EAM by targeting NF-κB of T cells during the inflammatory phase in EAM.

The present study showed for the first time that the IKK inhibitor IMD-0354 reduces the severity of EAM. This effect is associated with the reduction of inflammatory-related gene expression by inhibition of NF-κB activation. Some previous studies reported that administration of pharmacological agents indirectly inhibited NF-κB activation and suppressed the progression of EAM (1, 14, 40). Therefore, the IKK inhibitor IMD-0354, which directly inhibits NF-κB activation, may be promising as a therapeutic drug for the treatment of myocarditis. It is noteworthy that the IKK inhibitor will be clinically available in the near future. IMD-1041, which is a prodrug of IMD-0354, also inhibits IKK-β in vivo and in vitro (6).

Because this compound is an investigational drug, it is not yet on the market. To prove the clinical effect of IMD-1041, we started an interventional, randomized, placebo control and double blind clinical trial. Thus the IKK inhibitor will be used to treat myocarditis and other cardiovascular diseases in clinical settings in the future. Our data clearly indicate that IKK is critical for EAM development and its inhibition has significant effects for treating myocardial inflammation. In conclusion, IKK regulation is promising in the treatment of clinical acute myocarditis.

ACKNOWLEDGMENTS

We thank Noriko Tamura and Yasuko Matsuda for excellent technical assistance.

GRANTS

This study was supported by Takeda Science Foundation, Suzuken Memorial Foundation, a grant from the Research Foundation for Pharmaceutical Sciences, and the Japan Society for the Promotion of Science through its Funding Program for World-Leading Innovative R & D on Science and Technology (FIRST Program).

DISCLOSURES

No conflicts of interest, financial or otherwise, are declared by the author(s).

AUTHOR CONTRIBUTIONS

Author contributions: R.W., R.W.A., J.-i.S., and A.I. conception and design of research; R.W. and R.W.A. performed experiments; R.W. and R.W.A. analyzed data; R.W., R.W.A., J.-i.S., M.O., and M.I. interpreted results of experiments; R.W. prepared figures; R.W. drafted manuscript; R.W., J.-i.S., M.O., and M.I. edited and revised manuscript; R.W., J.-i.S., M.O., A.I., Y.H., I.K., and M.I. approved final version of manuscript.

REFERENCES

1. **Azuma RW, Suzuki J, Ogawa M, Futamatsu H, Koga N, Onai Y, Kosuge H, Isobe M.** HMG-CoA reductase inhibitor attenuates experimental autoimmune myocarditis through inhibition of T cell activation. *Cardiovasc Res* 64: 412–420, 2004.
2. **Barnes PJ, Karin M.** Nuclear factor-kappaB: a pivotal transcription factor in chronic inflammatory diseases. *N Engl J Med* 336: 1066–1071, 1997.
3. **Batra AS, Lewis AB.** Acute myocarditis. *Curr Opin Pediatr* 13: 234–239, 2001.
4. **Brechmann M, Mock T, Nickles D, Kiessling M, Weit N, Breuer R, Muller W, Wabnitz G, Frey F, Nicolay JP, Booken N, Samstag Y, Klemke CD, Herling M, Boutros M, Krammer PH, Arnold R.** A PP4 holoenzyme balances physiological and oncogenic nuclear factor-kappa B signaling in T lymphocytes. *Immunity* 37: 697–708, 2012.
5. **Corn RA, Aronica MA, Zhang F, Tong Y, Stanley SA, Kim SR, Stephenson L, Enerson B, McCarthy S, Mora A, Boothby M.** T cell-intrinsic requirement for NF-kappa B induction in postdifferentiation IFN-gamma production and clonal expansion in a Th1 response. *J Immunol* 171: 1816–1824, 2003.
6. **Fukuda S, Horimai C, Harada K, Wakamatsu T, Fukasawa H, Muto S, Itai A, Hayashi M.** Aldosterone-induced kidney injury is mediated by NF-κB activation. *Clin Exp Nephrol* 15: 41–49, 2011.
7. **Fuse K, Kodama M, Aizawa Y, Yamaura M, Tanabe Y, Takahashi K, Sakai K, Miida T, Oda H, Higuma N.** Th1/Th2 balance alteration in the clinical course of a patient with acute viral myocarditis. *Jpn Circ J* 65: 1082–1084, 2001.
8. **Fuse K, Kodama M, Ito M, Okura Y, Kato K, Hanawa H, Aoki S, Aizawa Y.** Polarity of helper T cell subsets represents disease nature and clinical course of experimental autoimmune myocarditis in rats. *Clin Exp Immunol* 134: 403–408, 2003.
9. **Futamatsu H, Suzuki J, Kosuge H, Yokoseki O, Kamada M, Ito H, Inobe M, Isobe M, Uede T.** Attenuation of experimental autoimmune myocarditis by blocking activated T cells through inducible costimulatory molecule pathway. *Cardiovasc Res* 59: 95–104, 2003.
10. **Futamatsu H, Suzuki J, Mizuno S, Koga N, Adachi S, Kosuge H, Maejima Y, Hirao K, Nakamura T, Isobe M.** Hepatocyte growth factor ameliorates the progression of experimental autoimmune myocarditis: a potential role for induction of T helper 2 cytokines. *Circ Res* 96: 823–830, 2005.
11. **Goser S, Ottl R, Brodner A, Dengler TJ, Torzewski J, Egashira K, Rose NR, Katus HA, Kaya Z.** Critical role for monocyte chemoattractant protein-1 and macrophage inflammatory protein-1alpha in induction of experimental autoimmune myocarditis and effective anti-monocyte chemoattractant protein-1 gene therapy. *Circulation* 112: 3400–3407, 2005.
12. **Granelli-Piperno A, Nolan P.** Nuclear transcription factors that bind to elements of the IL-2 promoter. Induction requirements in primary human T cells. *J Immunol* 147: 2734–2739, 1991.
13. **Haas GJ.** Etiology, evaluation, and management of acute myocarditis. *Cardiol Rev* 9: 88–95, 2001.
14. **Haga T, Suzuki J, Kosuge H, Ogawa M, Saiki H, Haraguchi G, Maejima Y, Isobe M, Uede T.** Attenuation of experimental autoimmune myocarditis by blocking T cell activation through 4–1BB pathway. *J Mol Cell Cardiol* 46: 719–727, 2009.
15. **Hamaya R, Ogawa M, Kobayashi N, Suzuki J, Itai A, Hirata Y, Nagai R, Isobe M.** A novel IKK inhibitor prevents progression of restenosis after arterial injury in mice. *Int Heart J* 53: 133–138, 2012.
16. **Hernandez-Presa M, Bustos C, Ortego M, Tunon J, Renedo G, Ruiz-Ortega M, Egido J.** Angiotensin-converting enzyme inhibition prevents arterial nuclear factor-kappa B activation, monocyte chemoattractant protein-1 expression, and macrophage infiltration in a rabbit model of early accelerated atherosclerosis. *Circulation* 95: 1532–1541, 1997.
17. **Inayama M, Nishioka Y, Azuma M, Muto S, Aono Y, Makino H, Tani K, Uehara H, Izumi K, Itai A, Sone S.** A novel IκB kinase-beta inhibitor ameliorates bleomycin-induced pulmonary fibrosis in mice. *Am J Respir Crit Care Med* 173: 1016–1022, 2006.
18. **Ivashkiv LB.** Inflammatory signaling in macrophages: transitions from acute to tolerant and alternative activation states. *Eur J Immunol* 41: 2477–2481, 2011.
19. **Kamon J, Yamauchi T, Muto S, Takekawa S, Ito Y, Hada Y, Ogawa W, Itai A, Kasuga M, Tobe K, Kadowaki T.** A novel IKKbeta inhibitor stimulates adiponectin levels and ameliorates obesity-linked insulin resistance. *Biochem Biophys Res Commun* 323: 242–248, 2004.
20. **Kang H, Moon JY, Sohn NW.** Regulation of interferon-gamma, interleukin-4 and interleukin-2 by Schizonepeta tenuifolia through differential effects on nuclear factor-kappaB, NFATc2 and STAT4/6. *Exp Biol Med (Maywood)* 235: 230–236, 2010.
21. **Kodama M, Matsumoto Y, Fujiwara M.** In vivo lymphocyte-mediated myocardial injuries demonstrated by adoptive transfer of experimental autoimmune myocarditis. *Circulation* 85: 1918–1926, 1992.
22. **Kodama M, Zhang S, Hanawa H, Shibata A.** Immunohistochemical characterization of infiltrating mononuclear cells in the rat heart with experimental autoimmune giant cell myocarditis. *Clin Exp Immunol* 90: 330–335, 1992.
23. **Leuschner F, Katus HA, Kaya Z.** Autoimmune myocarditis: past, present and future. *J Autoimmun* 33: 282–289, 2009.
24. **Leuschner F, Panizzi P, Chico-Calero I, Lee WW, Ueno T, Cortez-Retamozo V, Waterman P, Gorbatov R, Marinelli B, Iwamoto Y, Chudnovskiy A, Figueiredo JL, Sosnovik DE, Pittet MJ, Swirski FK, Weissleder R, Nahrendorf M.** Angiotensin-converting enzyme inhibition prevents the release of monocytes from their splenic reservoir in mice with myocardial infarction. *Circ Res* 107: 1364–1373, 2010.
25. **Liu W, Li WM, Gao C, Sun NL.** Effects of atorvastatin on the Th1/Th2 polarization of ongoing experimental autoimmune myocarditis in Lewis rats. *J Autoimmun* 25: 258–263, 2005.
26. **Maisel A, Cesario D, Baird S, Rehman J, Haghighi P, Carter S.** Experimental autoimmune myocarditis produced by adoptive transfer of splenocytes after myocardial infarction. *Circ Res* 82: 458–463, 1998.
27. **Matsui Y, Inobe M, Okamoto H, Chiba S, Shimizu T, Kitabatake A, Uede T.** Blockade of T cell costimulatory signals using adenovirus vectors prevents both the induction and the progression of experimental autoimmune myocarditis. *J Mol Cell Cardiol* 34: 279–295, 2002.
28. **Ngoc PB, Suzuki J, Ogawa M, Hishikari K, Takayama K, Hirata Y, Nagai R, Isobe M.** The anti-inflammatory mechanism of prostaglandin e2 receptor 4 activation in rat experimental autoimmune myocarditis. *J Cardiovasc Pharmacol* 57: 365–372, 2011.

29. **Niederberger E, Geisslinger G.** The IKK-NF-kappaB pathway: a source for novel molecular drug targets in pain therapy? *FASEB J* 22: 3432–3442, 2008.
30. **Oakley CM.** Myocarditis, pericarditis and other pericardial diseases. *Heart* 84: 449–454, 2000.
31. **Ogawa H, Azuma M, Muto S, Nishioka Y, Honjo A, Tezuka T, Uehara H, Izumi K, Itai A, Sone S.** IkappaB kinase beta inhibitor IMD-0354 suppresses airway remodelling in a Dermatophagoides pteronyssinus-sensitized mouse model of chronic asthma. *Clin Exp Allergy* 41: 104–115, 2011.
32. **Ogawa M, Suzuki J, Takayama K, Senbonmatsu T, Hirata Y, Nagai R, Isobe M.** Impaired post-infarction cardiac remodeling in chronic kidney disease is due to excessive renin release. *Lab Invest* 92: 1766–1776, 2012.
33. **Okura Y, Yamamoto T, Goto S, Inomata T, Hirono S, Hanawa H, Feng L, Wilson CB, Kihara I, Izumi T, Shibata A, Aizawa Y, Seki S, Abo T.** Characterization of cytokine and iNOS mRNA expression in situ during the course of experimental autoimmune myocarditis in rats. *J Mol Cell Cardiol* 29: 491–502, 1997.
34. **Onai Y, Suzuki J, Kakuta T, Maejima Y, Haraguchi G, Fukasawa H, Muto S, Itai A, Isobe M.** Inhibition of IkappaB phosphorylation in cardiomyocytes attenuates myocardial ischemia/reperfusion injury. *Cardiovasc Res* 63: 51–59, 2004.
35. **Onai Y, Suzuki J, Maejima Y, Haraguchi G, Muto S, Itai A, Isobe M.** Inhibition of NF-κB improves left ventricular remodeling and cardiac dysfunction after myocardial infarction. *Am J Physiol Heart Circ Physiol* 292: H530–H538, 2007.
36. **Perez Leiros C, Goren N, Sterin-Borda L, Borda ES.** Myocardial dysfunction in an experimental model of autoimmune myocarditis: role of IFN-γ. *Neuroimmunomodulation* 4: 91–97, 1997.
37. **Savvatis K, van Linthout S, Miteva K, Pappritz K, Westermann D, Schefold JC, Fusch G, Weithauser A, Rauch U, Becher PM, Klingel K, Ringe J, Kurtz A, Schultheiss HP, Tschope C.** Mesenchymal stromal cells but not cardiac fibroblasts exert beneficial systemic immunomodulatory effects in experimental myocarditis. *PLos One* 7: e41047, 2012.
38. **Sica A, Dorman L, Viggiano V, Cippitelli M, Ghosh P, Rice N, Young HA.** Interaction of NF-kappaB and NFAT with the interferon-gamma promoter. *J Biol Chem* 272: 30412–30420, 1997.
39. **Smith SC, Allen PM.** Myosin-induced acute myocarditis is a T cell-mediated disease. *J Immunol* 147: 2141–2147, 1991.
40. **Suzuki J, Ogawa M, Futamatsu H, Kosuge H, Sagesaka YM, Isobe M.** Tea catechins improve left ventricular dysfunction, suppress myocardial inflammation and fibrosis, and alter cytokine expression in rat autoimmune myocarditis. *Eur J Heart Fail* 9: 152–159, 2007.
41. **Suzuki J, Ogawa M, Muto S, Itai A, Isobe M, Hirata Y, Nagai R.** Novel IkB kinase inhibitors for treatment of nuclear factor-kB-related diseases. *Expert Opin Investig Drugs* 20: 395–405, 2011.
42. **Tanaka T, Ogawa M, Suzuki J, Sekinishi A, Itai A, Hirata Y, Nagai R, Isobe M.** Inhibition of IκB phosphorylation prevents load-induced cardiac dysfunction in mice. *Am J Physiol Heart Circ Physiol* 303: H1435–H1445, 2012.
43. **Ueda A, Okuda K, Ohno S, Shirai A, Igarashi T, Matsunaga K, Fukushima J, Kawamoto S, Ishigatsubo Y, Okubo T.** NF-kappa B and Sp1 regulate transcription of the human monocyte chemoattractant protein-1 gene. *J Immunol* 153: 2052–2063, 1994.
44. **Verweij CL, Geerts M, Aarden LA.** Activation of interleukin-2 gene transcription via the T-cell surface molecule CD28 is mediated through an NF-κB-like response element. *J Biol Chem* 266: 14179–14182, 1991.
45. **Wakatsuki S, Suzuki J, Ogawa M, Masumura M, Muto S, Shimizu T, Takayama K, Itai A, Isobe M.** A novel IKK inhibitor suppresses heart failure and chronic remodeling after myocardial ischemia via MMP alteration. *Expert Opin Ther Targets* 12: 1469–1476, 2008.
46. **Wu JL, Matsui S, Zong ZP, Nishikawa K, Sun BG, Katsuda S, Fu M.** Amelioration of myocarditis by statin through inhibiting cross-talk between antigen presenting cells and lymphocytes in rats. *J Mol Cell Cardiol* 44: 1023–1031, 2008.
47. **Yokoseki O, Suzuki J, Kitabayashi H, Watanabe N, Wada Y, Aoki M, Morishita R, Kaneda Y, Ogihara T, Futamatsu H, Kobayashi Y, Isobe M.** cis Element decoy against nuclear factor-kappaB attenuates development of experimental autoimmune myocarditis in rats. *Circ Res* 89: 899–906, 2001.
48. **Yoshida T, Hanawa H, Toba K, Watanabe H, Watanabe R, Yoshida K, Abe S, Kato K, Kodama M, Aizawa Y.** Expression of immunological molecules by cardiomyocytes and inflammatory and interstitial cells in rat autoimmune myocarditis. *Cardiovasc Res* 68: 278–288, 2005.
49. **Zee-Cheng CS, Tsai CC, Palmer DC, Codd JE, Pennington DG, Williams GA.** High incidence of myocarditis by endomyocardial biopsy in patients with idiopathic congestive cardiomyopathy. *J Am Coll Cardiol* 3: 63–70, 1984.

ELSEVIER

Brain & Development 36 (2014) 180–182

BRAIN & DEVELOPMENT
Official Journal of the Japanese Society of Child Neurology

www.elsevier.com/locate/braindev

Case report

MELAS phenotype associated with m.3302A>G mutation in mitochondrial tRNA$^{Leu(UUR)}$ gene

Masahide Goto[a], Hirofumi Komaki[a,*], Takashi Saito[a], Yoshiaki Saito[a], Eiji Nakagawa[a], Kenji Sugai[a], Masayuki Sasaki[a], Ichizo Nishino[b], Yu-ichi Goto[c]

[a] *Department of Child Neurology, National Center Hospital, National Center of Neurology and Psychiatry, Tokyo, Japan*
[b] *Department of Neuromuscular Research, National Institute of Neuroscience, National Center of Neurology and Psychiatry, Tokyo, Japan*
[c] *Department of Mental Retardation and Birth Defect Research, National Institute of Neuroscience, National Center of Neurology and Psychiatry, Tokyo, Japan*

Received 26 March 2012; received in revised form 31 January 2013; accepted 13 March 2013

Abstract

The m.3302A>G mutation in the mitochondrial tRNA$^{Leu(UUR)}$ gene has been identified in only 12 patients from 6 families, all manifesting adult-onset slowly progressive myopathy with minor central nervous system involvement. An 11-year-old boy presented with progressive proximal-dominant muscle weakness from age 7 years. At age 10, he developed recurrent stroke-like episodes. Mitochondrial myopathy, encephalopathy, lactic acidosis, plus stroke-like episodes (MELAS) was diagnosed by clinical symptoms and muscle biopsy findings. Mitochondrial gene analysis revealed a heteroplasmic m.3302A>G mutation. Histological examination showed strongly SDH reactive blood vessels (SSVs), not present in previous cases with myopathies due to the m.3302A>G mutation. These findings broaden the phenotypic spectrum of this mutation.

Keywords: MELAS; Myopathy; m.3302A>G mutation

1. Introduction

The m.3302A>G mutation in the mitochondrial tRNA$^{Leu(UUR)}$ gene was identified in 6 families including 12 patients with adult-onset slowly progressive myopathy and minor central nervous system complications including hearing disabilities and oculomotor symptoms [1–4]. In contrast, we experienced a child harboring the same mutation who showed the mitochondrial encephalopathy, lactic acidosis, plus stroke-like episodes (MELAS) phenotype. Approximately 80% of MELAS cases are caused by an A-to-G transition mutation at position 3243 in the mitochondrial tRNA$^{Leu(UUR)}$ (MTTL1) gene [5]. The relationship of this mutation to the MELAS phenotype is noteworthy.

2. Case report

A 7-year-old boy presented with gait disturbance and progressive proximal-dominant muscle weakness. He had normal psychomotor development until the development of the symptoms. His maternal members including his mother did not have symptoms associated with mitochondrial diseases such as short stature, diabetes mellitus, hearing loss, mental retardation, and cardiac complication. Generalized seizures emerged at age 10 years, subsequently occurring 8 times within one year. Electroencephalography revealed sporadic sharp

* Corresponding author. Address: Department of Child Neurology, National Center Hospital, National Center of Neurology and Psychiatry (NCNP), 4-1-1 Ogawahigashi-cho, Kodaira, Tokyo 187-8551, Japan. Tel.: +81 42 341 2711; fax: +81 42 344 6745.
E-mail address: komakih@ncnp.go.jp (H. Komaki).

0387-7604/$ - see front matter
http://dx.doi.org/10.1016/j.braindev.2013.03.001

Table 1
Laboratory data.

Serum		(Normal range)	
Creatine kinase	716	(57–197)	IU/L
Lactate	68.4	(3.0–17.0)	mg/dL
Pyruvate	1.60	(0.3–0.94)	mg/dL
Cerebrospinal fluid			
Lactate	44.0	(8.4–16.6)	mg/dL
Pyruvate	1.92	(0.63–1.27)	mg/dL

waves at mid-frontal areas. On physical examination at age 11 years, he showed winged scapulas and proximal muscle weakness necessitated Gowers' maneuver to stand. His deep tendon reflexes were decreased. Cranial nerve findings were unremarkable. IQ testing (WISC-III) revealed borderline mental retardation (full IQ 76). Serum creatine kinase, lactate and pyruvate, as well as cerebrospinal lactate and pyruvate, were elevated (Table 1).

Histological examination of biopsied muscle showed 30% of muscle to be ragged-red fibers (RRFs) by modified Gomori-trichrome staining. Succinate dehydrogenase (SDH) staining revealed strongly SDH reactive blood vessels (SSVs). Cytochrome c oxidase (COX) staining demonstrated variable enzyme activities from strongly positive to negative. Both RRFs and SSVs showed variable COX activities.

Respiratory chain enzyme activities in biopsied tissues were measured using previously reported methods [6]. The ratio of muscle complex I/II activities was markedly reduced to 12% of control values. Those of complex III/II and IV/II activities were 43% and 40%, respectively. In myoblasts and fibroblasts, these ratios were all within control ranges (Table 2).

Mitochondrial gene analysis was conducted as described elsewhere [7], and identified the m.3302A>G mutation located within the coding sequence of $tRNA^{Leu(UUR)}$. The heteroplasmy proportion of the m.3302A>G mutation was determined for each tissue by real-time PCR method using Taq-Man® probe on ABI 7700 according to the manufacturer. Mutation loads were $89.5 \pm 0.3\%$ in biopsied muscle, $85.8 \pm 0.7\%$ in myoblasts, $86.9 \pm 0.8\%$ in fibroblasts and $36.1 \pm 2.3\%$ in white blood cells.

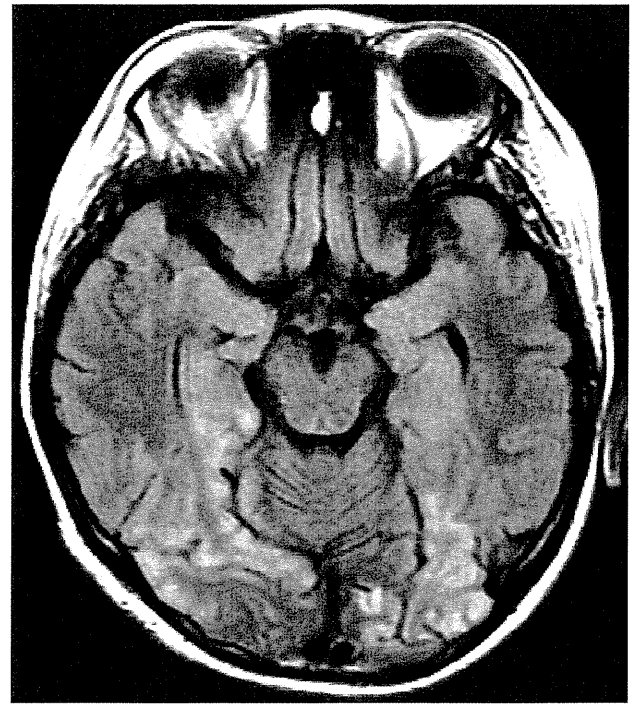

Fig. 1. Brain magnetic resonance imaging of the patient (fluid-attenuated inversion recovery imaging). Bilateral occipital lesions with high signal intensity are noted, whose distribution in not conforming to that of vascular territories.

After MELAS was diagnosed, the patient experienced stroke-like episodes with headache, vomiting, and occasionally cortical blindness. Brain magnetic resonance imaging (MRI) showed bilateral occipital lesions, confined to the cortical ribbon and not conforming to the distribution of vascular territories, with high signal intensity on fluid-attenuated inversion recovery images (Fig. 1). During the follow-up period, repeated MRI examinations never had basal ganglia lesions. At age 12 years, he became wheelchair-bound, and was nocturnal mask-medicated ventilator dependent due to chronic respiratory insufficiency.

Table 2
Respiratory chain enzyme activities.

Complex	Skeletal muscle		Myoblasts		Fibroblasts	
	Patient	Control ($n = 5$)	Patient	Control ($n = 5$)	Patient	Control ($n = 4$)
I/II	0.09	0.26–1.2	3.2	1.3–5.6	2	1.6–3.4
	12%	(0.76 ± 0.39)		(3.0 ± 1.7)		(2.0 ± 0.9)
III/II	0.39	0.72–1.8	3.4	3.2–7.4	5.3	1.9–5.6
	43%	(0.91 ± 0.41)		(4.2 ± 1.6)		(3.5 ± 1.8)
IV/II	0.35	0.42–1.3	3.7	2.1–9.1	2.8	2.2–5.0
	40%	(0.88 ± 0.36)		(4.7 ± 3.1)		(3.3 ± 1.2)

Complex I, III and IV activities are shown as proportions to that of complex II. Control values are expressed as mean ± standard deviation.

3. Discussion

Our patient initially manifested muscle weakness, developing epilepsy and stroke-like episodes years later. Elevated cerebrospinal lactate and pyruvate and bilateral occipital lesions with high signal intensity on MRI characterize the MELAS phenotype, and an m.3302A>G mutation was identified for the first time. The mutation was in a heteroplasmic state, a common feature of pathogenic mtDNA mutations. The significant tissue-to-tissue variability and inability to quantify the tissue specific mutational burden for the brain make it difficult to determine a prognosis for individuals harboring this mutation. Although the percentage of mutation load in differ little from those of in myoblast and fibroblast, the degree of the enzymatic deficiency in muscle, myoblasts, and fibroblasts are diverse in our patient. The threshold effects of this mutation might be different between muscle, fibroblasts and myoblasts.

However, the proportion of mutated mtDNA was highest in leptomeningeal and cortical blood vessel walls in all brain regions in a patient with severe COX deficiency [8]. Since mitochondrial dysfunction in vessels is assumed to be essential in the pathogenesis of stroke-like episodes in MELAS, such heteroplasmy may have been present in our patient. Moreover, although some cases with adult-onset slowly progressive mitochondrial myopathy with m.3302A>G mutations had hearing loss, recurrent headaches, ptosis, progressive external ophthalmoplegia, and depression [3], muscle biopsy revealed RRFs but no SSVs in these cases. Since SSVs represent an increased proportion of mutant mtDNA in vessel walls and are characteristic of MELAS [9,10], the SSVs in muscle tissue might be linked to the brain lesions through abundant mutated mtDNA in blood vessels in the central nervous system in our patient.

His maternal members including his mother did not have symptoms associated with mitochondrial diseases. It would have been useful that we analyze their heteroplasmic conditions, however, we could not obtain the samples of his maternal members because of the disapproval of providing the samples.

In conclusion, our case suggested the m.3302A>G mutation to cause the clinical MELAS phenotype. We should pay attention to headache, convulsion and other symptoms suggesting MELAS in patients with mitochondrial myopathies, particularly those with SSVs on muscle pathology.

Acknowledgments

This work was partly supported by Research Grant (21A-6) for Nervous and Mental Disorders (YG and EN) and Grants-in-Aid for Research on Intractable Diseases (Mitochondrial Disease) (YG and HK) from the Ministry of Health, Labour and Welfare of Japan. We thank Dr. Yutaka Nonoda, and Dr. Hideyuki Hatakeyama, Dr. Chika Sakai, Ms. Mayuko Kato and Ms. Yoshie Sawano for technical assistance.

References

[1] Bindoff LA, Howell N, Poulton J, McCullough DA, Morten KJ, Lightowlers RN, et al. Abnormal RNA processing associated with a novel tRNA mutation in mitochondrial DNA. A potential disease mechanism. J Biol Chem 1993;268:19559–64.
[2] van den Bosch BJ, de Coo IF, Hendrickx AT, Busch HF, de Jong G, Scholte HR, et al. Increased risk for cardiorespiratory failure associated with the A3302G mutation in the mitochondrial DNA encoded $tRNA^{Leu(UUR)}$ gene. Neuromuscul Disord 2004;14:683–8.
[3] Hutchison WM, Thyagarajan D, Poulton J, Marchington DR, Kirby DM, Manji SS, et al. Clinical and molecular features of encephalomyopathy due to the A3302G mutation in the mitochondrial $tRNA^{Leu(UUR)}$ gene. Arch Neurol 2005;62:1920–3.
[4] Ballhausen D, Guerry F, Hahn D, Schaller A, Nuoffer JM, Bonafé L, et al. Mitochondrial tRNALeu(UUR) mutation m.3302A>G presenting as childhood-onset severe myopathy: threshold determination through segregation study. J Inherit Metab Dis, in press. doi:10.1007/s10545-010-9098-2.
[5] Schaefer AM, McFarland R, Blakcly EI, He L, Whittaker RG, Taylor RW, et al. Prevalence of mitochondrial DNA disease in adults. Ann Neurol 2008;63:35–9.
[6] Trounce LA, Kim YL, Jun AS, Wallace DC. Assessment of mitochondrial oxidative phosphorylation in patient muscle biopsies, lymphoblasts, and transmitochondrial cell lines. In: Attardi GM, Chomyn A, editors. Methods in enzymology, vol. 264. San Diego, USA: Academic Press; 1996. p. 484–509.
[7] Akanuma J, Muraki K, Komaki H, Nonaka I, Goto Y. Two pathogenic point mutations exist in the authentic mitochondrial genome, not in the nuclear pseudogene. J Hum Genet 2000;45:337–41.
[8] Betts J, Jaros E, Perry RH, Schaefer AM, Taylor RW, Abdel-All Z, et al. Molecular neuropathology of MELAS: level of heteroplasmy in individual neurons and evidence of extensive vascular involvement. Neuropathol Appl Neurobiol 2006;32:359–73.
[9] Hasegawa H, Matusoka T, Goto Y, Nonaka I. Strongly succinate dehydrogenase-reactive blood vessels in muscles from patients with mitochondrial myopathy, encephalopathy, lactic acidosis, and stroke-like episodes. Ann Neurol 1991;29:601–5.
[10] Goto Y. Clinical features of MELAS and mitochondrial DNA mutations. Muscle Nerve 1995;3:S107–12.

Am J Physiol Heart Circ Physiol 305: H295–H304, 2013.
First published May 24, 2013; doi:10.1152/ajpheart.00990.2012.

CALL FOR PAPERS *Mitochondria in Cardiovascular Physiology and Disease*

Glucagon-like peptide-1 receptor activation reverses cardiac remodeling via normalizing cardiac steatosis and oxidative stress in type 2 diabetes

Akio Monji,* Toko Mitsui,* Yasuko K. Bando, Morihiko Aoyama, Toshimasa Shigeta, and Toyoaki Murohara

Department of Cardiology, Nagoya University Graduate School of Medicine, Nagoya, Japan

Submitted 31 December 2012; accepted in final form 15 May 2013

Monji A, Mitsui T, Bando YK, Aoyama M, Shigeta T, Murohara T. Glucagon-like peptide-1 receptor activation reverses cardiac remodeling via normalizing cardiac steatosis and oxidative stress in type 2 diabetes. *Am J Physiol Heart Circ Physiol* 305: H295–H304, 2013. First published May 24, 2013; doi:10.1152/ajpheart.00990.2012.—Glucagon-like peptide-1 receptor (GLP-1R) agonist exendin-4 (Ex-4) is a remedy for type 2 diabetes mellitus (T2DM). Ex-4 ameliorates cardiac dysfunction induced by myocardial infarction in preclinical and clinical settings. However, it remains unclear whether Ex-4 may modulate diabetic cardiomyopathy. We tested the impact of Ex-4 on two types of diabetic cardiomyopathy models, genetic (KK) and acquired T2DM induced by high-fat diet [diet-induced obesity (DIO)], to clarify whether Ex-4 may combat independently of etiology. Each type of mice was divided into Ex-4 (24 nmol·kg^{-1}·day^{-1} for 40 days; KK-ex4 and DIO-ex4) and vehicle (KK-v and DIO-v) groups. Ex-4 ameliorated systemic and cardiac insulin resistance and dyslipidemia in both T2DM models. T2DM mice exhibited systolic (DIO-v) and diastolic (DIO-v and KK-v) left ventricular dysfunctions, which were restored by Ex-4 with reduction in left ventricular hypertrophy. DIO-v and KK-v exhibited increased myocardial fibrosis and steatosis (lipid accumulation), in which were observed cardiac mitochondrial remodeling and enhanced mitochondrial oxidative damage. Ex-4 treatment reversed these cardiac remodeling and oxidative stress. Cytokine array revealed that Ex-4-sensitive inflammatory cytokines were ICAM-1 and macrophage colony-stimulating factor. Ex-4 ameliorated myocardial oxidative stress via suppression of NADPH oxidase 4 with concomitant elevation of antioxidants (SOD-1 and glutathione peroxidase). In conclusion, GLP-1R agonism reverses cardiac remodeling and dysfunction observed in T2DM via normalizing imbalance of lipid metabolism and related inflammation/oxidative stress.

diabetes mellitus; mitochondria; oxidative stress; glucagon-like peptide-1; insulin resistance

GLUCAGON-LIKE PEPTIDE-1 RECEPTOR (GLP-1R) agonist is one of the remedies for type 2 diabetes mellitus (T2DM) used for patients at an advanced stage in which refractory cases to oral hypoglycemic reagents (4). In addition to its therapeutic action on diabetic condition, accumulating evidence demonstrated that GLP-1R agonism ameliorates systolic dysfunction in preclinical (2, 22) and clinical heart failure after ischemic heart disease (3, 20). Furthermore, recent reports have demonstrated the GLP-1 analog liraglutide ameliorates liver (19) and cardiac steatosis via modulation on the endoplasmic reticulum (ER) stress (24) in diet-induced obesity (DIO) mice. However, to our knowledge, it remains unclear whether the GLP-1R agonism may ameliorate cardiac remodeling and dysfunction observed in T2DM.

Suggested cardiac remodeling observed in overnutrition, such as obesity and T2DM, is illustrated by the histologic characteristics, i.e., cardiac fibrosis, myocardial hypertrophy, and steatosis of myocardium (29), at least in part, because of lipotoxity to heart (36). The presence of overnutrition results in alterations in not only systemic but also cardiac insulin resistance (6), fatty acid transport/storage/oxidation, oxygen consumption, and redox status, leading to the mitochondrial damages and subsequent maladaptive cardiac remodeling and dysfunction (5, 6, 36); however, it remains unclear whether systemic intervention by GLP-1R agonism for the overnutrition state may concomitantly reverse the relevant cardiac remodeling and dysfunction.

Accordingly, we hypothesized whether the GLP-1R activator exendin-4 (Ex-4) may mitigate cardiac dysfunction and remodeling occurred in T2DM by ameliorating cardiac oxidative stress that was presumably induced by concomitant steatosis and/or enhanced insulin resistance. To elucidate this notion more universally, we tested the impact of Ex-4 on diabetic heart by used of 2 distinct T2DM models, genetic and acquired T2DM induced by high-fat diet (HFD; DIO).

METHODS

Mice models. All procedures involving mice were approved by the Institutional Animal Care and Use Committee of Nagoya University. Two types of T2DM models were allocated: genetic T2DM model (KKAy) (14, 35) and age- and sex-matched (male)-acquired T2DM mice fed with high-fat diet (HFD60, Oriental Yeast, Tokyo, Japan) (32). Mice were allocated into experimental groups as follows: Ex-4 (24 nmol·kg^{-1}·day^{-1}, subcutaneously administrated by osmotic pump for 40 days; KK-ex4 and DIO-ex4; Sigma-Aldrich) and vehicle groups (KK-v and DIO-v). The overview of experimental protocol regarding mice feeding and drug treatment that applied to the present study was displayed in Fig. 1. The food consumption was measured by weighing new and remaining food three times weekly according to the previous report (19). Changes in food intake of individual mouse was expressed as the average value of food intake that was calculated from daily food intake for the whole experimental course. Oral glucose tolerance test was performed as follows: mice were subjected 6 h fasting, and glucose (2 g/kg body wt) was orally administered. Changes in blood glucose level were measured using the handy glucometer system (Sanwa-Kagaku, Nagoya, Japan) at the time point of 0, 30, 60, and 120 min after the glucose loading.

Blood chemistry. Blood glucose level was measured through a tail nick using a handheld glucometer. Plasma cholesterol and triglyceride

* A. Monji and T. Mitsui equally contributed to this work.
Address for reprint requests and other correspondence: Y. K. Bando, Dept. of Cardiology, Nagoya Univ. Graduate School of Medicine, 65 Tsurumai-cho, Showa-ku, Nagoya, Aichi, 466-8550, Japan (e-mail: ybando@med.nagoya-u.ac.jp).

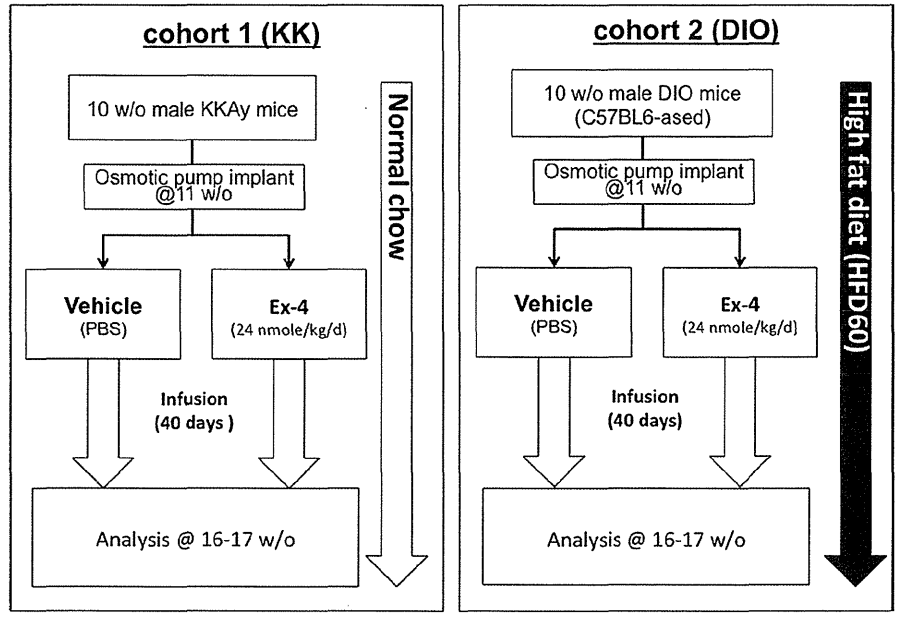

Fig. 1. Experimental protocol. Two cohorts of diabetic mouse models were allocated in the present study. *Cohort 1*, genetic type 2 diabetic model using KKAy (KK) mice; *cohort 2*, acquired type 2 diabetic mice induced by diet-induced obesity (DIO) mice of C57BL6 background. *Cohort 1* was fed with normal chow diet, and *cohort 2* was continuously fed with high-fat diet (60% fat content) to avoid diet-induced decline in body weight. w/o, without; d, day.

levels were measured using each blood specimen collected at the time of euthanizing from heart puncture of each mouse. Plasma insulin levels were determined by radioimmunoassay (Mouse Insulin RIA Kit; Millipore, MA).

Echocardiography. Cardiac function of each mouse was assessed using a complete two-dimensional and M-mode and Doppler echocardiogram [ACUSON Sequoia 512 system with a 15-MHz high-frequency transducer (Microson 15L8), Siemens]. Mice were anesthetized using a combination of ketamine (75 mg/kg) and xylazine (10 mg/kg) anesthesia to avoid any influence of the type of anesthesia on heart rate or left ventricular (LV) function (33).

Immunoblotting. Each heart tissue sample was subjected to frost shattering using Cryopress (Microtech Nichion, Chiba, Japan). Proteins were extracted in radioimmunoprecipitation assay buffer containing protease and phosphatase inhibitor cocktails. Equal amounts (10 μg) of protein from each group were electrophoresed and subjected to immunoblotting. Protein bands were detected using the following specific antibodies: phospho-insulin receptor substrate 1 (IRS-1) (Millipore), phospho-cAMP response element binding protein (CREB), GAPDH (Cell Signaling Technology), SOD-1 (Santa Cruz), and NADPH oxidases 4 (Nox4) and 2 (Nox2), glutathione peroxidase (GPx), and thioredoxin (TRx) (Abcam). The density of each protein band was analyzed using an image analysis software (ImageJ).

Cytokine array. A proteome profiler array was performed according to the manufacturer's instructions [Mouse Cytokine Array, Panel A (ARY006); R&D system, Minneapolis, MN]. In brief, after a 1-h membrane-blocking step, the preincubated mouse plasma-biotinylated antibody mixture was added, and the membrane was incubated overnight. After a series of washes, the membrane was incubated with horseradish peroxidase-conjugated streptavidin, and the signal was detected by using X-ray film. Average protein expression levels were measured by densitometry (ImageJ).

Immunohistochemistry and microscopic analysis. Frozen sections of heart tissue (8 μm) were subjected to immunohistochemistry and examined under a fluorescence microscope (Axio Observer Z1, Carl Zeiss MicroImaging). The cell surface area and ceramide accumulation in cardiomyocytes were detected using the following specific antibodies: dystrophin (Novocastra) and ceramide (Sigma), respectively. Each result was quantified by use of the ImageJ software as described previously (33).

Cardiac cAMP concentration. Frost-shattered heart samples using the Cryopress were subjected to cAMP concentration measurement using commercially available kit according to the manufacturer's protocols (Promega, WI).

Cardiac superoxide detection. For detection of cardiac superoxide radical levels, we used specific fluorescence dye dihydrothidium (DHE) as a probe (Invitrogen Molecular Probes). The sources of reactive oxygen species (ROS), including superoxide, are derived from mitochondrial respiratory chain and nonrespiratory chain origins (5, 28). To dissect out the source of ROS originated from mitochondrial respiratory chain, each heart section was pretreated with rotenone (100 μM), the inhibitor for mitochondrial electron chain complex I, and subjected to DHE staining (1 μM). To detect the mitochondria-specific oxidative stress level, each heart section was loaded

Table 1. *Effects of exendin-4 on body weight, heart weight, and glucose metabolism*

	KK-v	KK-ex4	DIO-v	DIO-ex4	CTL-v
BW, g	54 ± 1	52 ± 2	44 ± 1	35 ± 1	29 ± 1
HW, mg	223 ± 7	204 ± 8	140 ± 8	115 ± 1	136 ± 2
HW/BW	4.2 ± 0.2	3.7 ± 0.1	3.3 ± 0.1	3.3 ± 0.1	4.8 ± 0.1
BS, mg/dl	452 ± 114	468 ± 82	159 ± 14	143 ± 6	154 ± 23
Ins, μg/l	5.9 ± 0.5	2.9 ± 0.4*	3.1 ± 0.3	1.7 ± 0.4**	1.6 ± 0.3

Values are means ± SE; n = 3-10 for congenital type 2 diabetes mellitus mice (KK), and n = 3-9 for diet-induced obese mice. KK and DIO mice with vehicle treatment (KK-v and DIO-v, respectively) and the exendin-4 treated KK and DIO mice (KK-ex4 and DIO-ex4, respectively) and lean control mice (CTL) are shown. BW, body weight; BS, nonfasting blood sugar concentration; Ins, nonfasting plasma insulin concentration. $^{**}P < 0.01$ and $^{*}P < 0.05$ ves. vehicle counterpart.

with mitochondrial fluorescence probes mirotracker red (100 nM MTR; CM-H2XRos) in the presence of 200 nM mitotracker green, which is a carbocyanine-based mitochondrion-specific probe and detects all mitochondria by covalently binding to the inner mitochondrial membrane independently of membrane potential. MTR is nonfluorescent at baseline, and it becomes fluorescent once MTR is oxidized by ROS within mitochondria.

Transmission electron microscopy. Small pieces of LV myocardium were obtained from the LV free wall of adult male mice; fixed in Karnovsky's solution consisting of 2% paraformaldehyde, 2.5% glutaraldehyde, and 0.1 M phosphate buffer; and processed until embedding into epon plastic. Ultrathin sections were stained with 1% (wt/vol) uranyl acetate followed by Reynold's lead citrate. Micrographs were collected using a JEM-1400 transmission electron microscope (JEOL, Tokyo, Japan) at 100 kV and lower (×1,000) and higher (×5,000 and ×8,000) magnification. Scanned micrographs were analyzed using ImageJ software for the calculation of mitochondrial area and total mitochondrial number.

Mitochondrial fractionation. Frost-shattered heart samples using the Cryopress were subjected to mitochondrial fractionation using

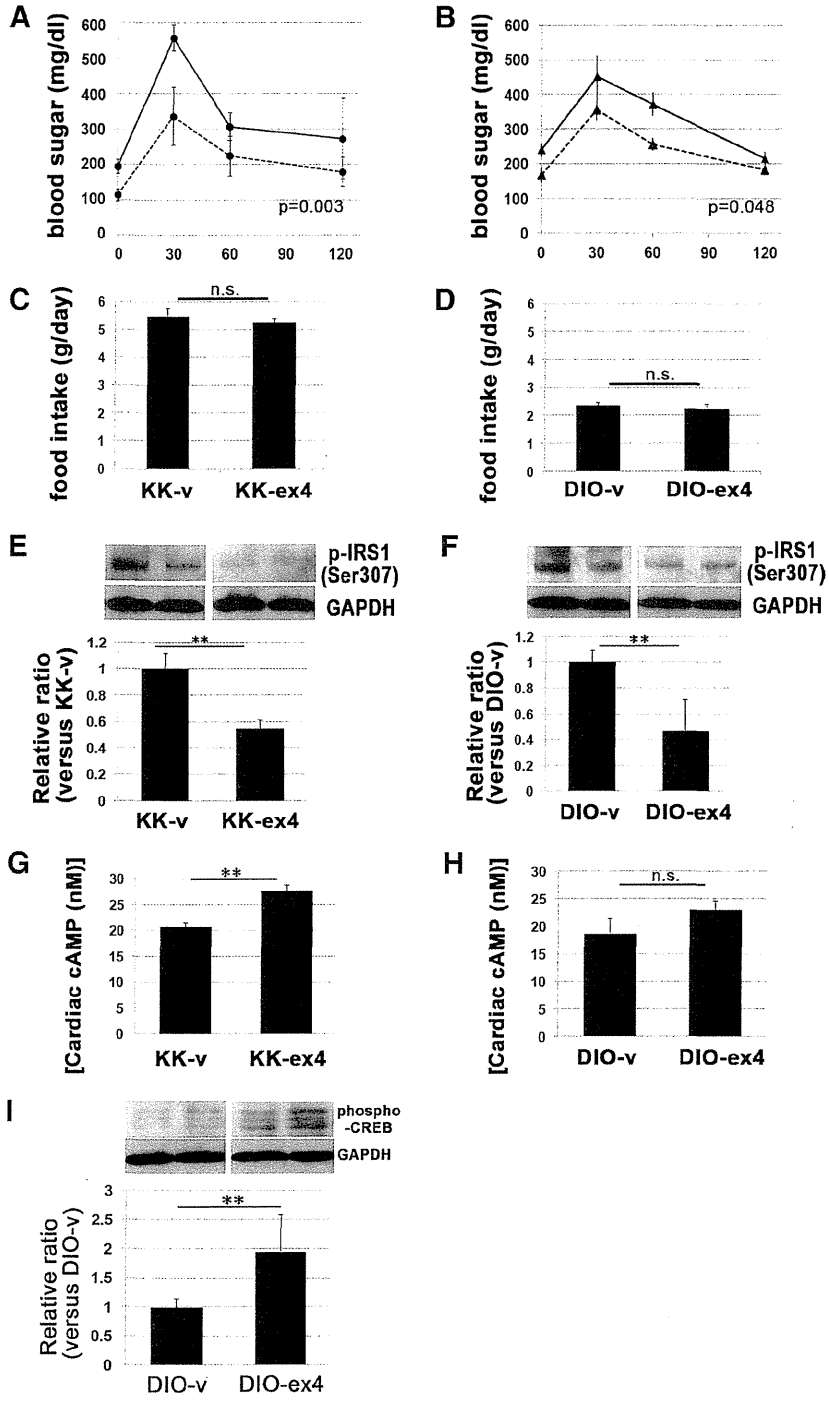

Fig. 2. Exendin-4 (Ex-4) ameliorated systemic and myocardial insulin resistance without affecting food intake. *A* and *B*: effect of Ex-4 treatment on impaired glucose tolerance in KKAy (*A*) and DIO (*B*) mice. Mice were subjected 6 h fasting, and glucose (2 g/kg body wt) was orally administered. Changes in blood glucose level were measured at the time point of 0, 30, 60, and 120 min after the glucose loading. Ex-4 ameliorated glucose tolerance both of KKAy ($P = 0.003$ by ANOVA) and DIO ($P = 0.048$ by ANOVA). *C* and *D*: mean of daily food intake of each mouse remain unchanged by administration of Ex-4. *E* and *F*: changes in cardiac insulin sensitivity were assessed by the phosphorylation level of insulin receptor substrate 1 (IRS-1). Increased IRS-1 phosphorylation levels indicates the impaired insulin sensitivity. *Left*: cardiac IRS-1 phosphorylation level of KKAy mice treated with vehicle (KK-v) and with Ex-4 (KK-ex4). *Right*: DIO with vehicle (DIO-v) and Ex-4 (DIO-ex4). Each panel of representative blot represents the results of 2 independent specimens obtained from the same group. GAPDH, internal control. *G* and *H*: effect of Ex-4 on cardiac cAMP concentrations in KKAy mice. The cAMP levels (in nM) were measured using each heart extract. *I*: changes in protein kinase A activity exhibited by the phospho-cAMP response element binding protein (CREB) level in DIO mouse hearts. $^{**}P < 0.01$ vs. vehicle counterpart ($n = 7$–10 for KK; $n = 4$–9 for DIO). ns, not significant.

density gradient procedure with commercially available kit (Pierce, Thermofisher Scientific), and each fraction was subjected to immunoblot analysis using antibodies of anti-Parkin (Abcam), anti-PTEN-induced kinase 1 (PINK1) (MerckMillipore, MA), anti-voltage-dependent anion channel (Abcam), anti-mitofusin-1 (Mfn1) (Santa Cruz, CA), and anti-Mfn2 (Sigma).

Statistical analyses. Data are expressed as means ± SE. Data analyses were performed using commercially available JMP software (JMP, version 8.0, SAS Institute). For comparisons between two groups, we employed Student's *t*-tests and ANOVA as appropriate. Values of $P < 0.05$ were considered statistically significant.

RESULTS

Ex-4 ameliorated systemic and myocardial insulin resistance and cardiac function without affecting food intake. Previous reports demonstrated GLP-1 analog liraglutide mitigates glucose intolerance and reduced heart mass without affecting body weight in mice (19, 24). We first examined the effects of Ex-4 on glucose homeostasis and changes in body and heart weight of KK and DIO mice (Table. 1). Ex-4 treatment ameliorated hyperinsulinemia and heart weight both in KK and DIO groups, whereas it had no effect on each body weight or postprandial blood glucose levels (19). To evaluate the impact of Ex-4 on systemic glucose intolerance more precisely, we performed oral glucose tolerance test, demonstrating that the 40-day Ex-4 treatment significantly ameliorated glucose intolerance both in KK (Fig. 2*A*) and DIO (Fig. 2*B*) without affecting the extent of food intake of each group (Fig. 2, *C* and *D*).

Impaired cardiac insulin signaling elicits mitochondrial damage leading to oxidative stress in heart, leading to cardiac remodeling and dysfunction (6). To further examine the effect of Ex-4 treatment on cardiac insulin sensitivity, we next assessed changes in phosphorylation level of IRS-1 (1) (Fig. 2, *E* and *F*). As expected, the cardiac IRS-1 phosphorylation levels were decreased both in KK-ex4 (Fig. 2*E*) and DIO-ex4 (Fig. 2*F*), suggesting that Ex-4 treatment ameliorated cardiac insulin resistance in those T2DM mice. Lastly, to confirm whether the systemic administration of Ex-4 may successfully act on heart, we measured cardiac cAMP concentration in each mouse heart, because GLP-1R activation generally promotes increase in intracellular cAMP level (10). Cardiac cAMP level was elevated in KK-ex4 compared with KK-v (Fig. 2*G*). In DIO-ex4 heart, we found the same trend of cAMP elevation; however, there was no statistical significance (Fig. 2*H*). We additionally examined the changes in cardiac phospho-CREB level of DIO-ex4, which is one of the surrogates for protein kinase A activation, and found marked elevation of phospho-CREB in DIO-ex4 heart (Fig. 2*I*). We next examined the impact of Ex-4 on cardiac function (Table 2) of each mouse. Echocardiography revealed that DIO-v exhibited systolic and diastolic LV dysfunction, which were restored by Ex-4 treatment with reduction in LV wall thickening. In KK-v, their systolic function remained unchanged, whereas those diastolic LV function was impaired and exhibited LV hypertrophy, which are consistent with characteristics to diabetic heart (5). Ex-4 reversed these diastolic dysfunction and LV hypertrophy of KK heart.

Ex-4 ameliorated cardiac remodeling observed in T2DM independently from etiology. We next examined the effects of Ex-4 on the cardiac remodeling induced by T2DM in terms of morphological changes (Fig. 3). Consistently with the findings observed in echocardiography (Table 2), histological analysis revealed that T2DM increased cardiomyocyte size, which was reversed by Ex-4 treatment (Fig. 3, *A* and *B*). Diabetic heart exhibits enhanced cardiac fibrosis (33, 39). We thus evaluated changes in cardiac fibrosis by Sirius red staining (Fig. 3, *C* and *D*). In KK-v and DIO-v, the Sirius red-positive fibrotic area was markedly increased, which were suppressed both in KK-ex4 (Fig. 3*C*) and DIO-ex4 groups (Fig. 3*D*).

We next examined the effects of Ex-4 on the cardiac mitochondrial remodeling observed in T2DM by transition electron microscopy (Fig. 3, *E–H*). In KK-v (Fig. 3*E*, *top*) and DIO-v (Fig. 3*F*, *top*), most mitochondrial cristae structure were destroyed and defragmented, leading to reduction in size (Fig. 3*G*) and increase in number (Fig. 3*H*). Ex-4 ameliorated those morphological changes of mitochondria both in KK and DIO mice (Fig. 3, *E–H*, *bottom*).

Ex-4 ameliorated cardiac mitochondrial remodeling observed in T2DM presumably via reduction of oxidative stress. To further clarify the effects of Ex-4 on the morphological changes of cardiac mitochondria detected by transition electron microscopy, we next conducted several experiments for detecting mitochondrial damage more specifically (Fig. 4). Because we found that both KK and DIO heart exhibited cardiac insulin resistance, which was reported to promote mitochondrial dysfunction and oxidative stress in the heart (6), we next hypothesized whether Ex-4 may ameliorate mitochondrial remodeling in diabetic heart via reduction of mitochondrial oxidative stress

Table 2. *Effects of exendin-4 on cardiac function of diabetic models*

	KK-v	KK-ex4	DIO-v	DIO-ex4	CTL-v
IVSd, mm	1.2 ± 0.1	1.0 ± 0.1*	1.1 ± 0.1	0.8 ± 0.1*	0.8 ± 0.1
LVPWd, mm	1.1 ± 0.1	1.0 ± 0.1*	1.0 ± 0.1	0.8 ± 0.1*	0.8 ± 0.1
LVDd, mm	3.7 ± 0.1	3.6 ± 0.1	3.6 ± 0.1	3.3 ± 0.2*	3.5 ± 0.1
LVDs, mm	2.3 ± 0.1	2.3 ± 0.1	2.5 ± 0.1	2.1 ± 0.1*	2.2 ± 0.1
EF, %	73 ± 1	72 ± 1	65 ± 1	74 ± 1**	73 ± 2
FS, %	37 ± 1	35 ± 1	30 ± 1	37 ± 1**	38 ± 2
E, m/s	0.8 ± 0.1	0.9 ± 0.1*	1.0 ± 0.1	1.2 ± 0.1*	0.8 ± 0.1
A, m/s	0.5 ± 0.1	0.4 ± 0.1	0.6 ± 0.1	0.6 ± 0.1	0.3 ± 0.1
E/*A* ratio	2.3 ± 0.1	2.8 ± 0.2**	1.6 ± 0.1	2.2 ± 0.2**	2.7 ± 0.1
DcT, ms	45 ± 1	37 ± 1*	43 ± 1	36 ± 1*	32 ± 2

Values are means ± SE; $n = 7$ for KK, and $n = 9$ for DIO. Systolic and diastolic left-ventricular (LV) functions were evaluated by echocardiogram. IVSd, diastolic interventricular septal wall thickness; LVPWd, diastolic LV posterior wall thickness; LVDd, diastolic LV diameter; LVDs, systolic LV diameter; EF, LV ejection fraction; FS, LV fraction shortening; *E*, mitral Doppler-flow velocity E wave; *A*, mitral Doppler-flow velocity A wave; Dct, deceleration time of mitral early inflow. **$P < 0.01$ and *$P < 0.05$ vs. vehicle counterpart.

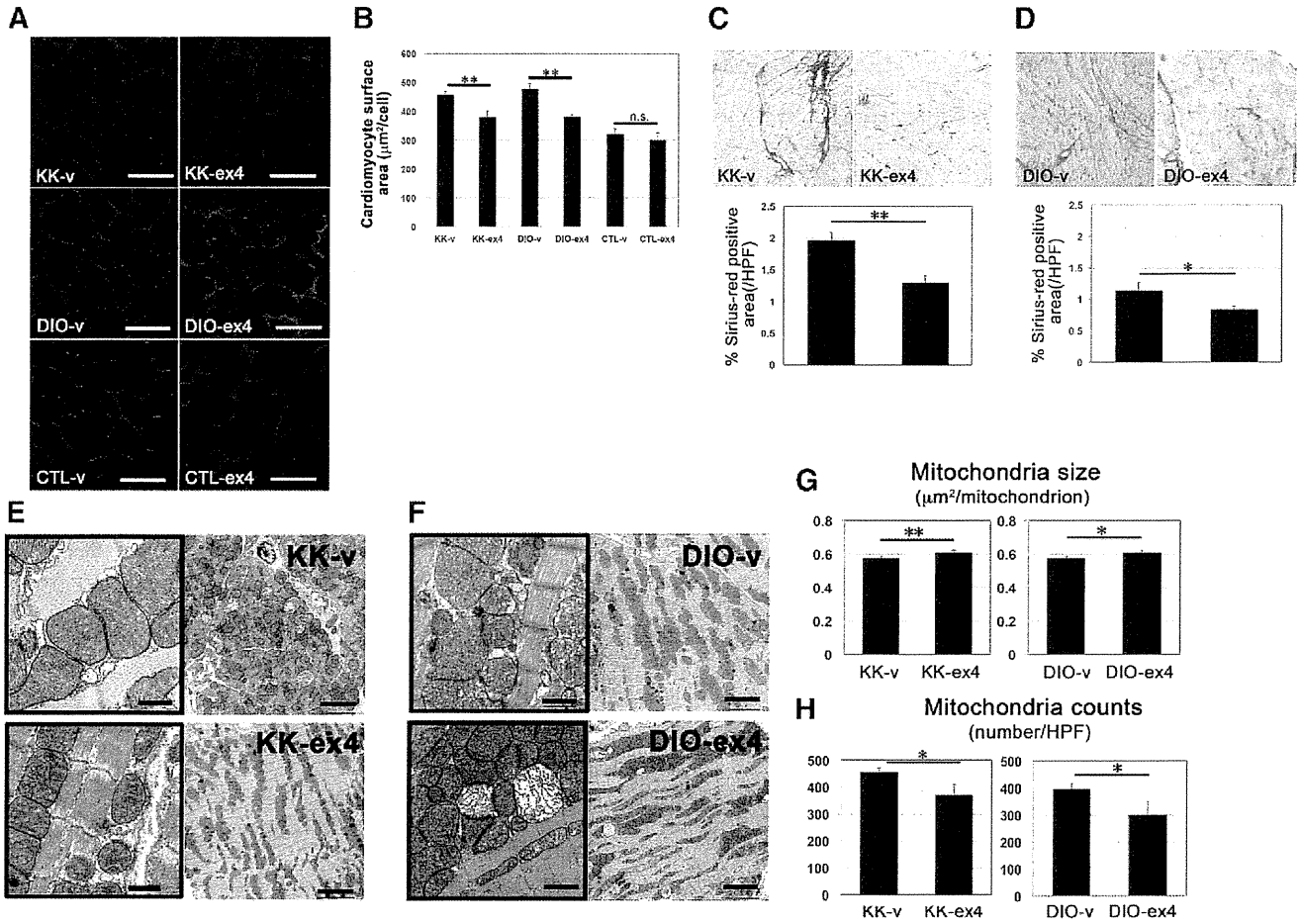

Fig. 3. Ex-4 reduced cardiomyocyte size and cardiac fibrosis and ameliorated mitochondrial remodeling in diabetic myocardium. Effects of Ex-4 on changes in cardiac remodeling assessed by histologic analysis. *A* and *B*: each cardiomyocyte surface area was detected by immunofluorescence using anti-dystrophin antibody (red, *A*). *Top*: heart sections obtained from KK-v (*left*) and KK-ex4 (*right*). *Middle*: DIO-v (*left*) and DIO-ex4 (*right*). *Bottom*: lean control (CTL-v, *right*) and lean mice treated with Ex-4 (CTL-ex4). *Bottom*: Ex-4-treated groups of KK (*left*), DIO (*middle*), and lean control (*right*). Data were summarized in bar graph. $^{**}P < 0.01$ vs. vehicle counterpart (n = 7–10). *C* and *D*: changes in cardiac fibrosis detected by Sirius-red staining. The Sirius-red-positive fibrotic area were measured by conversion of densitometric data and summarized in each graph represented below the representative images: KK-v and KK-ex4 (*C*), DIO-v and DIO-ex4 (*D*). $^{**}P < 0.01$ and $^{*}P < 0.05$ vs. vehicle counterpart (n = 7–10). *E–H*: effects of Ex-4 on mitochondrial remodeling observed in diabetic myocardium by transition electron microscopy (TEM). Each pair of TEM images displayed a set of higher magnification (*left*; scale bar, 1 μm) and those observed at a lower magnification (*right*; scale bar, 5 μm). *E*, *top*: KK-v heart. *E*, *bottom*: KK-ex4. *F*, *top*: DIO-v heart. *F*, *bottom*: DIO-ex4. *G* and *H*: summary of mitochondrial morphologic changes in TEM images. Bar graphs indicate mean mitochondria size (*G*) and counts (*H*) per lower magnification images. $^{*}P < 0.05$ (n = 4–6). HPF, high power field.

(Fig. 4, *A–C*). Mitotracker red (MTR), a useful indicator for mitochondria-specific oxidative stress level, revealed that the MTR-positive spots were markedly increased both of KK and DIO hearts compared with the nondiabetic counterpart (Fig. 4, *A–C*), which were diminished in Ex-4-treated mouse hearts [for KK (Fig. 4*A*, *left*) and DIO (Fig. 4*B*, *left*)].

Mfn1 and Mfn2 are mitochondrial regulatory proteins that determine mitochondria morphological changes and dynamics via regulating fission/fusion, and the endogenous levels of Mfn1 attenuate cardiomyocyte viability in the face of an imminent oxidative stress (ROS) observed in obesity (25). Using mitochondrial fractionation, we next examined changes in Mfn1 and Mfn2 levels as a probe for diabetes-mediated mitochondrial damage. Both of KK and DIO groups, their Mfn1/Mfn2 ratio was found to be reduced by Ex-4-treated groups (Fig. 4, *D* and *E*, *left*). We further confirmed the impact of Ex-4 on mitochondrial damage observed in T2DM heart by use of another surrogate for mitochondrial damage, PARKIN and PINK, of which complex accumulates specifically to the damaged mitochondria observed in a ROS-mediated mitophagy (12, 37). In KK-v (Fig. 4*F*) and DIO-v (Fig. 4*G*), both PARKIN and PINK1 levels were abundant in each mitochondrial fraction, which was reversed by Ex-4 treatment.

Ex-4 reduced cardiac lipid accumulation and inflammatory cytokines in T2DM. Obesity causes enhancing of not only oxidative stress but also local/systemic inflammation, which links obesity-related insulin resistance (13, 40). New evidence exploring the mechanisms linking ROS and inflammation find that ROS derived from mitochondria act as signal-transducing molecules that provoke the upregulation of inflammatory cytokines (21). Furthermore, ample evidence demonstrates that Ex-4 was reported to exert anti-inflammatory effects in human

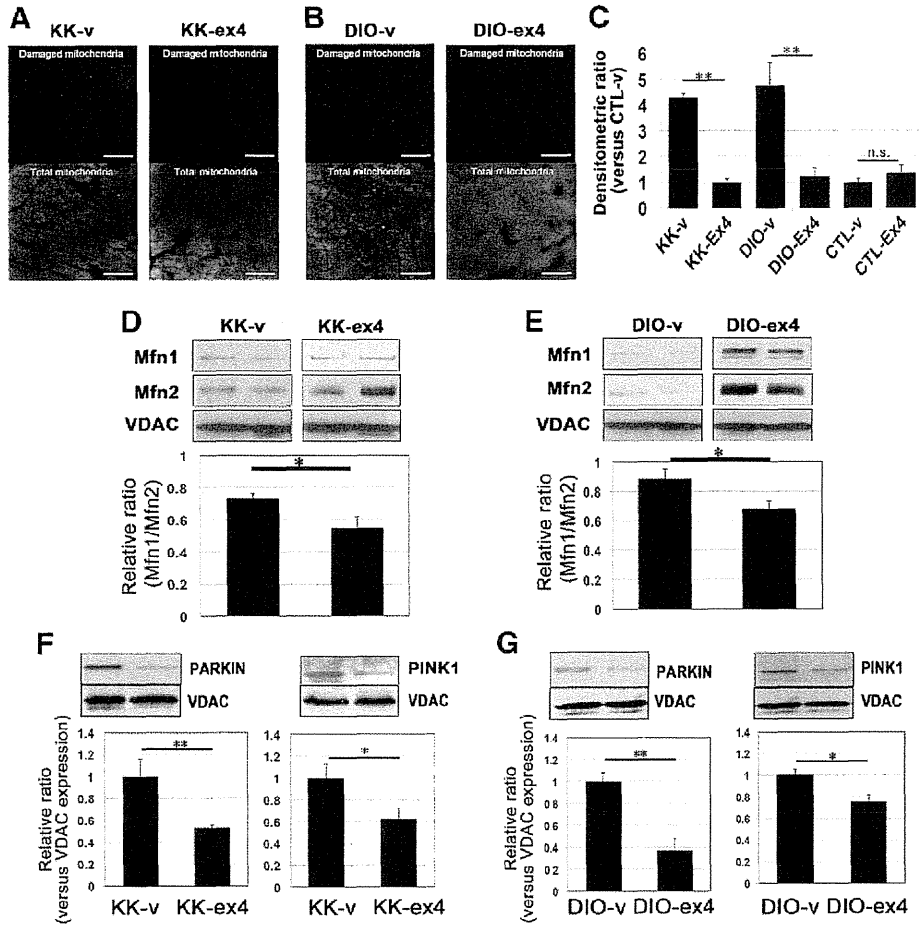

Fig. 4. Ex-4 ameliorated cardiac mitochondrial oxidative stress and damage in diabetic myocardium. *A* and *B*: mitochondria-specific oxidative stress was detected by mirotracker red (MTR, 100 nM) in the presence of mitotracker green (200 nM) as a control detecting total mitochondria. MTR becomes red once MTR is oxidized by reactive oxygen species within mitochondria: KK-v and KK-ex4 (*A*) and DIO-v and DIO-ex4 (*B*). Data were converted as densitometric ratio vs. CTL-v and summarized in bar graph (*C*). $^{**}P < 0.01$ and $^{*}P < 0.05$. *D–G*: protective effect of Ex-4 on mitochondrial damage. Changes in mitofusin 1 and 2 (Mfn1/2) ratio (*D* and *E*) and mitophagy modulator Parkin (PARKIN) and PTEN-induced kinase 1 (PINK) levels (*F* and *G*) were assessed using mitochondria fractionation of each heart extract. Densitometry data were summarized as the relative ratio vs. those voltage-dependent anion channel (VDAC) as an internal control of standard mitochondrial proteins. $^{**}P < 0.01$ and $^{*}P < 0.05$ vs. vehicle counterpart.

(7) and in apolipoprotien-E knockout mice (26), which was presumably mediated by its another effect on lipid metabolism (7, 26). We thus hypothesized whether the impact of Ex-4 on the pathological lipid profile in T2DM may play a key role in its protective effects on diabetic myocardial remodeling. To elucidate this notion, we next examined the effect of Ex-4 on systemic and local/cardiac accumulation of lipids. We measured changes in plasma cholesterol levels and found that Ex-4 treatment decreased both total cholesterol (Fig. 5*A*) and triglyceride (Fig. 5*B*) levels in KK and DIO groups. GLP-1R agonism reduces very low-density lipoprotein production and hepatic steatosis (26). We next hypothesized whether Ex-4 may reduce cardiac steatosis, thereby normalizing cardiomyocyte size that occurred in T2DM (Fig. 5, *C* and *D*). Changes in cardiac steatosis were detected by ceramide staining, revealing that we found higher lipid accumulation to the heart in KK-v group (Fig. 5, *C* and *D*, *right* and *middle*), which was reversed by Ex-4 treatment (Fig. 5, *C* and *D*, *left top* and *left middle*). We also evaluated local lipid accumulation by use of Oil-red-O staining, which was found to be less sensitive than the case observed in ceramide staining; however, the distribution pattern of lipid in each diabetic heart seemed patchy, not uniformly diffuse (Fig. 5, *E* and *F*). We next aimed to specify any inflammatory cytokine that may be sensitive to Ex-4 treatment by use of cytokine array (Fig. 5, *G* and *H*). Both in KK (Fig. 5*G*) and DIO (Fig. 5*H*), Ex-4 treatment markedly reduced ICAM-1 and macrophage colony-stimulating factor (M-CSF). Regarding TNF-α, one of the cytokines modulating insulin resistance (15), it remained unchanged; we further confirmed this trend by measuring the plasma TNF-α level of each mouse using ELISA (data not shown).

Effects of GLP-1 receptor activation on cardiac oxidative stress and mitochondrial damage. Lastly, we examined the impact of Ex-4 on cardiac oxidative stress using superoxide-specific fluorescence dye DHE that detects superoxide derived from not only mitochondrial respiratory chain but also non-respiratory chain origins (5, 28). The DHE staining revealed that Ex-4 treatment reduced cardiac oxidative stress both in KK (Fig. 6*A*) and DIO (Fig. 6*B*). We further evaluated the mechanism(s) underlying the Ex-4-mediated antioxidant effects in terms of oxidative regulators (Nox2 and Nox4, SOD-1, TRx, and GPx). We found that cardiac Nox4 level was downregulated by Ex-4 despite the Nox2 level that remained unchanged (Fig. 6, *C* and *D*) both in DIO and KK. Of note, all of the antioxidant proteins we evaluated were increased in DIO-ex4 (Fig. 6*D*); however, those counterparts of KK-ex4 remained unaffected (Fig. 6*C*).

DISCUSSION

To date, it is getting familiar that metabolic disorders due to overnutrition such as T2DM and obesity promote cardiac